North Aegean core complexes, the gravity spreading of a thrust wedge

Konstantinos Kydonakis, Jean-Pierre Brun, Dimitrios Sokoutis

AGU PUBLICATIONS

JGR

Journal of Geophysical Research: Solid Earth

RESEARCH ARTICLE
10.1002/2014JB011601

Key Points:
- We performed physical experiments on orogenic thrust wedges
- During the early phase of extension, strain localizes always near the backstop
- Core complex development is related to the initial geometry of the models

Correspondence to:
K. Kydonakis,
konstantinos.kydonakis@gmail.com

Citation:
Kydonakis, K., J.-P. Brun, and D. Sokoutis (2015), North Aegean core complexes, the gravity spreading of a thrust wedge, *J. Geophys. Res. Solid Earth*, *120*, doi:10.1002/2014JB011601.

Received 10 SEP 2014
Accepted 16 DEC 2014
Accepted article online 19 DEC 2014

North Aegean core complexes, the gravity spreading of a thrust wedge

Konstantinos Kydonakis[1], Jean-Pierre Brun[1], and Dimitrios Sokoutis[2,3]

[1]Géosciences Rennes, UMR 6118 CNRS, Université de Rennes 1, Rennes, France, [2]Faculty of Earth Science, Utrecht University, Utrecht, Netherlands, [3]Department of Geosciences, University of Oslo, Oslo, Norway

Abstract The North Aegean core complexes developed in middle Eocene soon after the end of continental block convergence and piling up of the Hellenic Thrust Wedge. They formed during back-arc extension, driven by the Hellenic slab rollback, at the back of the thrust wedge. A series of scaled laboratory experiments was performed to test whether the gravity spreading of a thrust wedge is a suitable process for the development of the North Aegean core complexes during back-arc extension. Wedge-shaped sand-silicon models with variable boundary displacement velocities and different geometries of the upper sand layer were used to study the effects of variations in wedge rheology on the pattern of extension. The models exemplify that extension, either distributed (wide rift mode) or localized (core complex mode), is always located at the wedge rear. Core complex development was favored in models with thicker brittle layer (higher frictional strength) and low stretching rate (lower ductile strength). Both core complex location at the wedge rear and detachment location and dip are interdependent and intrinsically related to the initial wedge shape of the extending system. The experimental model displays striking similarities with the extensional pattern of the North Aegean in terms of (i) location, size, and shape of core complexes as well as their sequence of development and (ii) detachment location and dip. We conclude that it is the initial wedge geometry of the system and the weak nature of the crust at the onset of extension that controlled the extensional pattern of the North Aegean domain.

1. Introduction

Soon after the discovery of metamorphic core complexes and of their significance in terms of crustal-scale extension in the Basin and Range of western United States [*Davis and Coney*, 1979; *Coney*, 1980; *Crittenden et al.*, 1980; *Wernicke*, 1981, 1985], they have been identified in many other orogenic domains of Alpine age [e.g., *Dewey*, 1988] or even older (e.g., Proterozoic [*Cosca et al.*, 1995], Caledonian [*Norton*, 1986; *Andersen et al.*, 1991], and Hercynian [*Van Den Driessche and Brun*, 1989; *Brun and Van Den Driessche*, 1994]). The concept of core complex was also adapted to mantle exhumation at mid-oceanic ridges [*Karson*, 1990; *Tucholke and Lin*, 1994]. Various aspects of their development have been investigated using numerical and physical modeling techniques [e.g., *Brun et al.*, 1994; *Tirel et al.*, 2004a, 2006, 2008; *Wijns et al.*, 2005; *Dyksterhuis et al.*, 2007; *Gessner et al.*, 2007; *Rey et al.*, 2009a, 2009b; *Huet et al.*, 2011a, 2011b; *Schenker et al.*, 2012], and almost three decades after the emergence of the concept, considerable progress has been made concerning the mechanisms that control their formation (see comprehensive review by *Whitney et al.* [2013]).

In the Aegean, core complexes developed during back-arc extension in two strikingly different tectonic settings, below and above the Vardar Suture Zone, in the Cyclades and in the Rhodope, respectively (Figure 1). The Central Cyclades Core Complex (CCCC), to the south, developed since lower Miocene and display evidence for partial melting within the exhumed domes [*Gautier et al.*, 1993; *Gautier and Brun*, 1994; *Jolivet and Brun*, 2010; *Jolivet et al.*, 2010; *Philippon et al.*, 2012] (Figure 1). In such a setting, thermal relaxation that follows a crustal thickening phase cannot account for the observed partial melting. Therefore, it can be argued that the Cycladic Blueschist Unit represents a continental block that has been delaminated from the downgoing slab and subsequently allowed to be quickly exhumed during slab rollback [*Brun and Faccenna*, 2008; *Tirel et al.*, 2013]. Under these circumstances, the continental block undergoes a strong and fast heating from below as its base comes into direct contact with the asthenosphere, favoring core complex development during still ongoing extension. On the other hand, the Rhodopean core complexes, to the north, developed earlier than the CCCC and correspond (i) to an alignment of medium-sized (width of 10–20 km in the direction of stretching) gneiss domes in southern Bulgaria-northern Greece

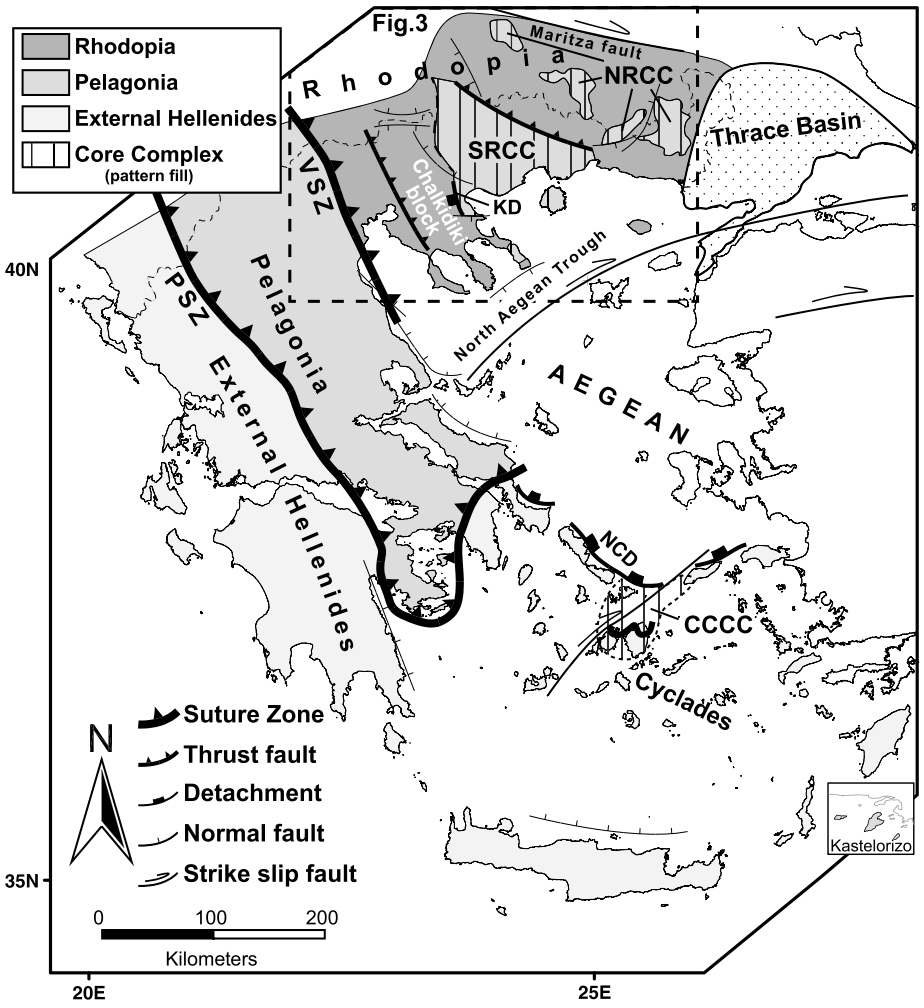

Figure 1. Simplified geological map of the Hellenides which are made, from north to south, of three continental blocks (Rhodopia, Pelagonia, and External Hellenides) and two intervening sutured oceanic domains (Vardar and Pindos Suture Zones). The Rhodopean and Cycladic Core Complexes are highlighted (pattern fill). CCCC: Central Cyclades Core Comple, KD: Kerdylion Detachment, NCD: North Cycladic Detachment, NRCC: Northern Rhodope Core Complex, PSZ: Pindos Suture Zone, SRCC: Southern Rhodope Core Complex, and VSZ: Vardar Suture Zone.

(see review in *Burg* [2012]) and (ii) to the Southern Rhodope Core Complex (SRCC) [*Sokoutis et al*., 1993; *Brun and Sokoutis*, 2007] that is a large structure (reaching 120 km in the direction of stretching in its southeast part) which started to develop during Eocene (Figure 1). Evidence for partial melting is also found within the exhumed Rhodopean gneiss domes. Another striking difference between the CCCC and the SRCC is the dip of the detachment responsible for their exhumation that is to the north for the first (North Cycladic Detachment [*Jolivet et al*., 2010]) and to the southwest for the second (Kerdylion Detachment [*Brun and Sokoutis*, 2007]).

While the development of the CCCC is rather well studied and understood, in the frame of slab rollback-driven extension of the Aegean, the origin of the Rhodopean core complexes raises a series of unsolved questions. Why they developed in two zones? Why they are located to the extreme northern part of the domain affected by the Aegean extension and they are separated from the Vardar Suture Zone by a block that remained undeformed until the Neogene? Why the Kerdylion Detachment that controlled exhumation of lower crust in the SRCC dips to the southwest? Using laboratory experiments presented in this paper, we argue that the gravity spreading of a thrust wedge stimulated by the slab rollback of the Hellenic subduction provides a straightforward answer to these questions.

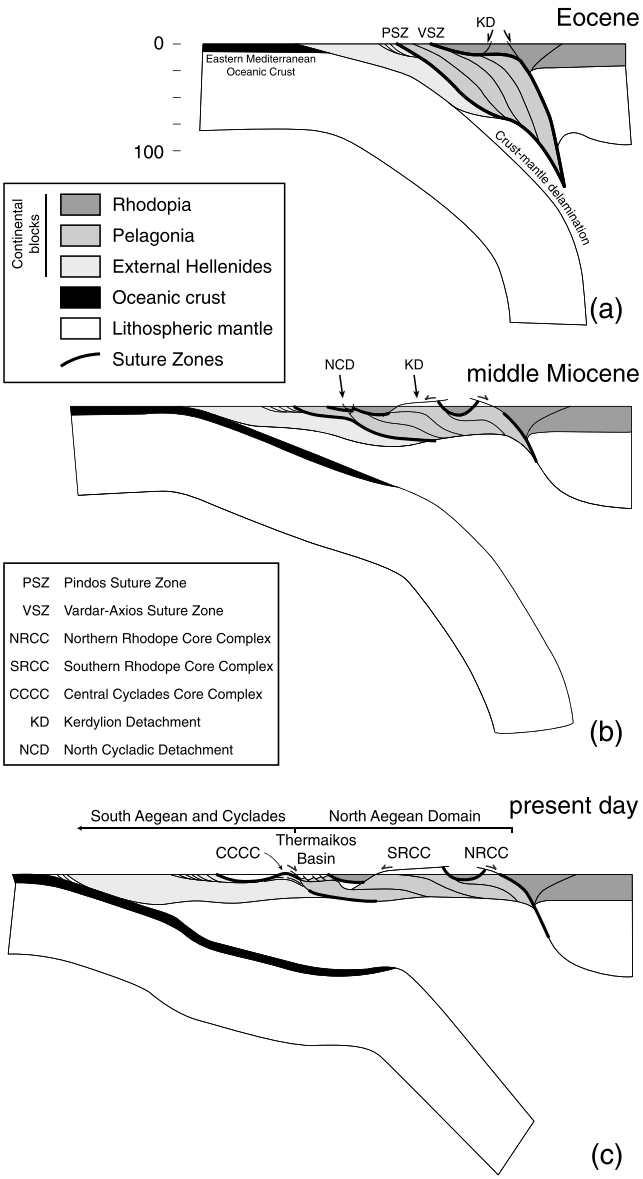

Figure 2. Lithospheric-scale cross-section restoration of the Hellenides. (a) In Eocene, the Hellenic Thrust Wedge was formed by the accretion of three continental blocks and two intervening sutures. The initial geometry of our models is scaled according to this time frame. (b) Subduction of the eastern Mediterranean oceanic domain, following crust-mantle delamination, allowed southward retreat of the Hellenic trench, upward movement of the accreted blocks, and subsequent development of the Rhodopean core complexes (NRCC and SRCC). (c) Present-day form of the Aegean.

2. North Aegean Tectonics

2.1. Aegean Extension

The Hellenides (Figure 1) constitute an integral part of the Alpine-Himalayan mountain chain and are the product of convergence between the stable south European margin and northward-driven Gondwana-derived continental blocks [e.g., *Dercourt et al*., 1993; *Stampfli and Borel*, 2002]. The Hellenides resulted from southwesterly piling up of three continental blocks (Rhodopia, Pelagonia, and External Hellenides). This process also involved the closure of the two intervening oceanic domains represented today by the Vardar-Axios (Vardar Suture Zone (VSZ)) and the Pindos Suture Zones (PSZ) in the north and south, respectively [*Robertson*, 2002; *van Hinsbergen et al*., 2005a; *Papanikolaou*, 2009, 2013] (Figures 1 and 2).

Seismic tomography illustrates in the Aegean region and down to 1600 km depth a northward dipping slab, anchored into the lower mantle [*Bijwaard et al*., 1998]. Aegean extension that started in middle Eocene was driven by the southward retreat of the Hellenic subduction zone [*McKenzie*, 1978; *Mercier et al*., 1979; *Mercier*, 1981; *Dewey and Sengör*, 1979; *Le Pichon and Angelier*, 1979, 1981; *Jolivet and Faccenna*, 2000] soon after the suturing of the Pindos oceanic domain [*Brun and Sokoutis*, 2010; *Jolivet and Brun*, 2010].

In the Aegean, evidence for extension since middle Eocene include (i) the migration of plutonic activity from the Rhodope to the southern Cyclades, (ii) exhumation of high-pressure metamorphic rocks in the southern Hellenides (Cyclades, Peloponnese, and Crete), and (iii) core complex formation in the Rhodope and the Cyclades. Since middle Miocene, extension resulted in widespread development of continental and marine sedimentary basins (see recent reviews of *Jolivet and Faccenna* [2000], *Burchfiel et al*. [2008], *Brun and Sokoutis* [2010], *Jolivet and Brun* [2010], *Ring et al*. [2010], *Royden and Papanikolaou* [2011], and *Jolivet et al*. [2013]).

During extension, the western part of the extending domain, from Rhodope to Peloponnese, has undergone up to 50°–60° clockwise rotation around an axis located in the vicinity of the Scutary-Pec in Albania [*Kissel and Laj*, 1988; *van Hinsbergen et al*., 2005b]. In this kinematic setting, the amount of extension increased (i) as a function of the distance from the rotation axis and (ii) from north to south [*Brun and Sokoutis*, 2010]. The

Aegean Sea that represents the more strongly stretched part of the back-arc domain is the result of a southward trench retreat of around 600–700 km [*Jolivet and Brun*, 2010]. In the Aegean, the Moho is rather flat over a distance of over 1000 km in north-south direction, and the crustal thickness has a mean value of 25 ± 2 km except in two structures, namely, the North Aegean Through and the Cretan Sea, where the crust is locally thinner than 22 km [*Tirel et al*., 2004b].

2.2. Tectonic History of the North Aegean

The domain of North Aegean forms the hinterland of the Hellenic subduction zone, where the early Jurassic-Cretaceous convergence history is recorded [e.g., *Burg et al*., 1990, 1995, 1996; *Ricou et al*., 1998]. It can be divided, from northeast to southwest, into the Northern Rhodope Domain (NRD), the Southern Rhodope Core Complex (SRCC), the Chalkidiki block, the Vardar s.l. Units (including the Vardar Complex and the Vardar Suture Zone), and the Pelagonia (Figures 1 and 3). The NRD and the Chalkidiki block form together the Rhodopia. The domain of North Aegean is bordered to the north by the Maritza dextral strike-slip fault, to the east by the middle Eocene to Quaternary Thrace Basin, to the west by the Vardar-Axios Suture Zone and the Pelagonia, and to the south by the Thermaikos Basin and the North Aegean Through (Figure 3).

From Upper Cretaceous to middle Eocene, the successive closure of the Vardar and Pindos oceanic domains led to the piling up of Rhodopia, Pelagonia, and External Hellenides and the formation of the Hellenic Thrust Wedge (Figure 2a). In Eocene, the thrust wedge was submitted to extension, likely related to the entrance of the eastern Mediterranean oceanic lithosphere into the subduction zone, leading to the formation of core complexes (Figures 2b and 2c). In the North Aegean domain, the latter are (i) the aligned extensional metamorphic domes of Chepinska, Arda, Kesebir-Kardamos, and Biela-Reka-Kechros to the northeast [*Burg*, 2012] that will be called hereafter as Northern Rhodope Core Complex (NRCC) for convenience and (ii) the Southern Rhodope Core Complex (SRCC) to the southwest [*Brun and Sokoutis*, 2007]. It must be noted here that whereas the larger SRCC is associated to the well-defined and southwest dipping Kerdylion Detachment, the extensional domes constituting the NRCC are not clearly connected to a single detachment (Figure 3). Field observations show top-to-north and top-to-south senses of shear with the former dominating over the latter shear sense (J.-P. Burg, personal communication). As these domes, which are rather small, are not connected to each other, they likely correspond to core complexes aborted at an early stage of development, prior to detachment localization at regional scale (see numerical models of *Tirel et al*. [2004a, 2008]).

The development of the SRCC separated Rhodopia in two main blocks: the NRD, to the northeast, and Chalkidiki block, to the southwest (Figure 3). In other words, the Southern Rhodope Core Complex is a tectonic window inside Rhodopia that exposes Pelagonia at the surface. During the exhumation of the SRCC, the Chalkidiki block, as part of the hanging wall of the Kerdylion Detachment, underwent an ~30° clockwise rotation [*Kondopoulou and Westphal*, 1986]. A southwestwardly migration of the extension from Paleogene to Neogene can be inferred from the deposition age of sediments and/or volcanic activity centers that becomes younger toward the southwest.

The tectonic history of the northern onshore part of the Aegean is summarized in map view in three selected time frames shown in Figure 4: (i) In lower Eocene (Figure 4a), the Northern Rhodope Domain and the Chalkidiki block are still attached forming Rhodopia. The two core complexes (NRCC and SRCC) initiated in Eocene. (ii) In lower Miocene, whereas the NRCC is already sealed by Paleogene sediments and volcanics, the SRCC is still exhuming (Figure 4b). (iii) From middle Miocene to present day (Figure 4c), extensional Neogene basins developed over the southern part of North Aegean hiding a large part of the SRCC and sealing the Kerdylion Detachment.

3. Modeling the Rotational Gravity Spreading of a Brittle-Ductile Thrust Wedge

3.1. Experimental Strategy

The conception of the modeling work that we present here is based on the present-day geological setting of the onshore part of the North Aegean and on our understanding of its tectonic history (previous section), including the physical processes involved. Our modeling strategy of back-arc extension that is based around the gravitational collapse [*Dewey*, 1988] of a brittle-ductile wedge does not consider the effects of toroidal mantle flow [e.g., *Funiciello et al*., 2003] and trench suction [e.g., *Conrad and Lithgow-Bertelloni*, 2002] that

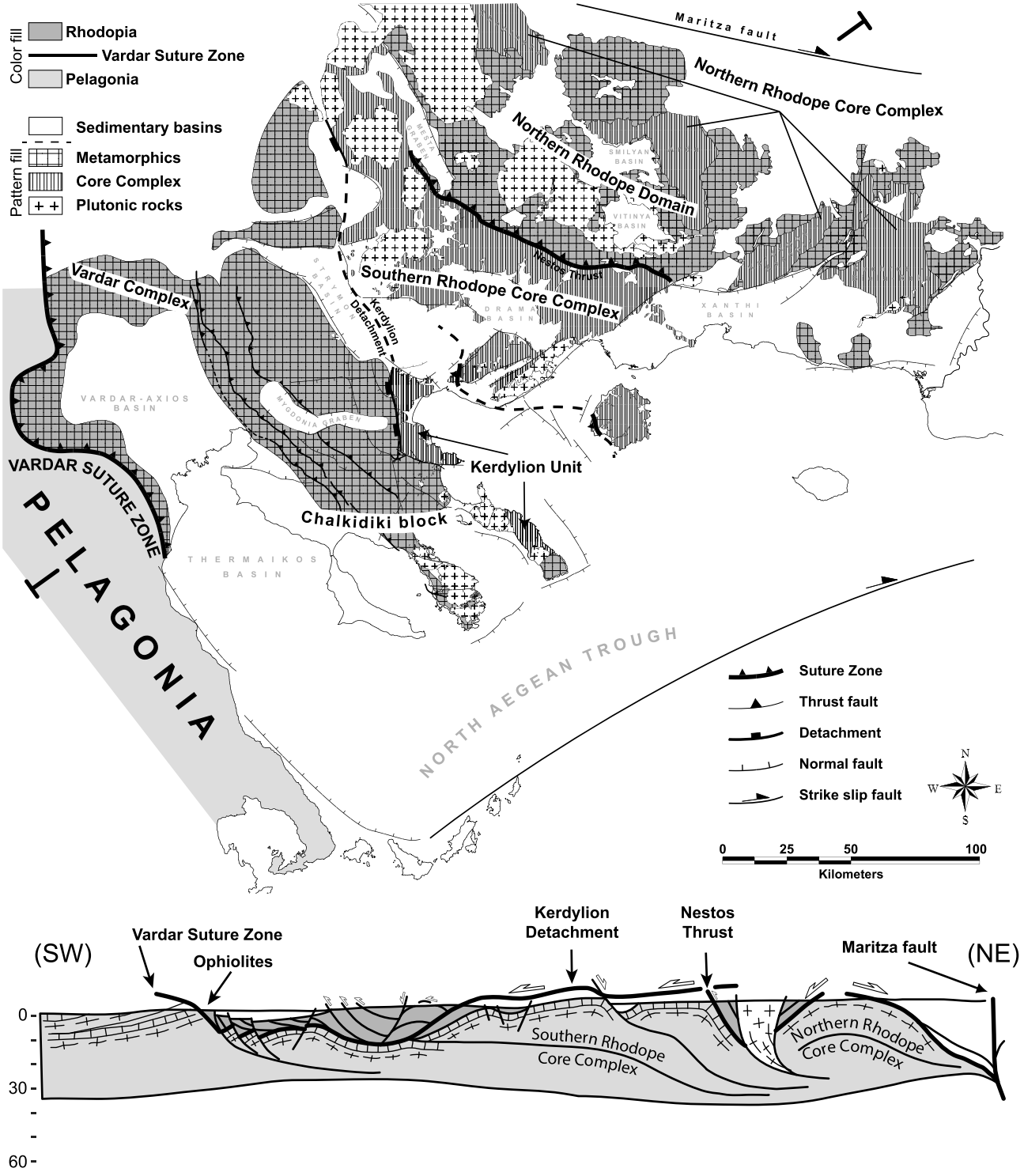

Figure 3. Simplified geological map of the North Aegean domain redrawn mostly after *Brun and Sokoutis* [2007] and *Burg* [2012] with particular interest on the core complexes cropping out in the area. Different tectonic domains can be distinguished, from northeast to southwest: (i) the Northern Rhodope Domain (NRD), (ii) the Southern Rhodope Core Complex (SRCC), (iii) the Chalkidiki block, (iv) the Vardar s.l. units, and (v) the Pelagonia. The term Northern Rhodope Core Complex (NRCC) is proposed here to be used collectively for the exhumed gneiss domes (Chepinska, Arda, Kardamos-Kesebir, and Kechros-Biela-Reka domes) exposed to the northeast within the NRD (see also Figure 4), whereas the term Southern Rhodope Core Complex (SRCC) [*Brun and Sokoutis*, 2007] is adopted for the triangle-shaped gneiss dome exposed at the central part of the map.

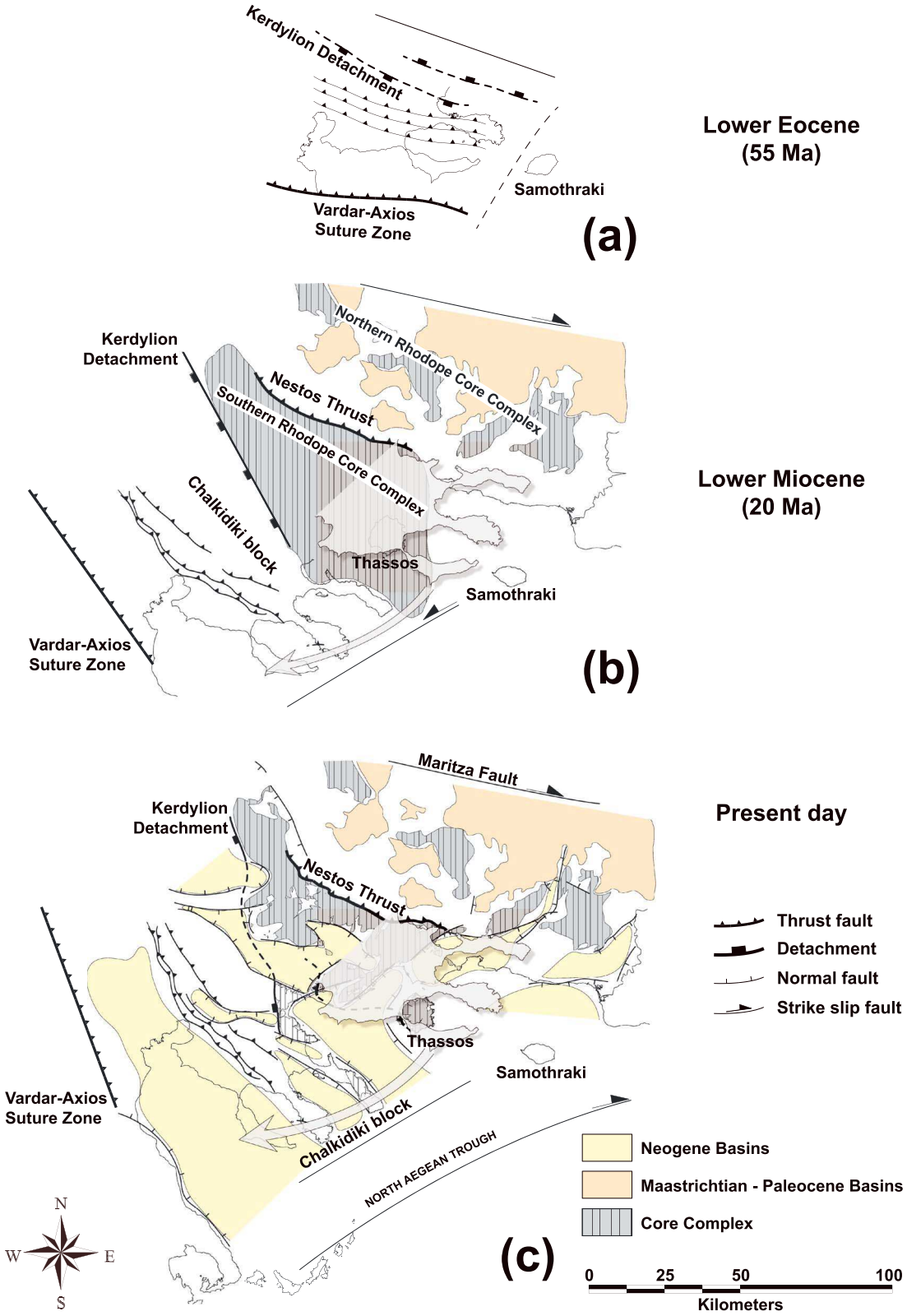

Figure 4. Map restoration of the North Aegean domain. Three key snapshots are shown between lower Eocene and the present day. Basin fill of Maastrichtian-Paleocene age is in close proximity to the NRCC, to the north, whereas younger basins were developed farther to the southwest by middle Miocene recording, overall, a southward swift of the extension. The exhumation of the SRCC facilitated by clockwise rotation of the Chalkidiki block. For reference, the Chalkidiki block is superimposed on the subfigures. See text for details.

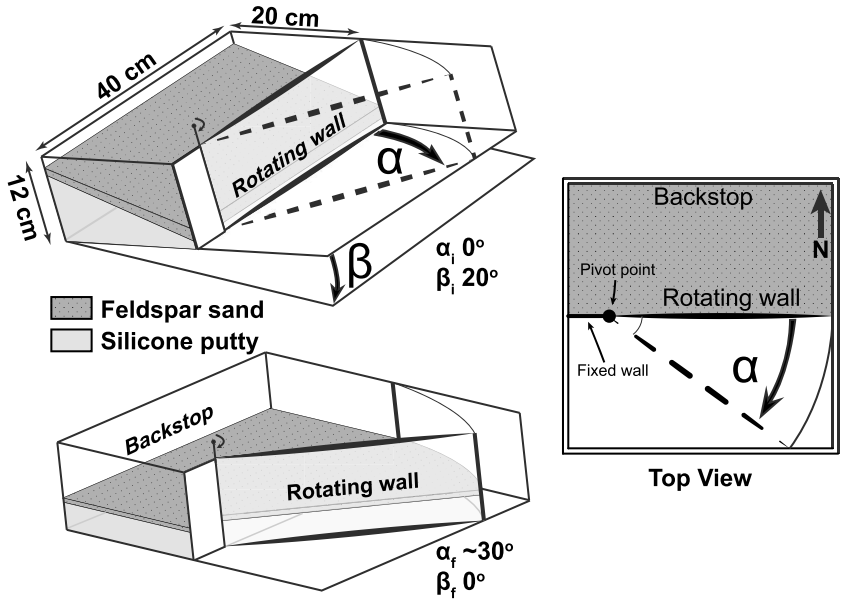

Figure 5. The experiments were performed in a Plexiglas box using feldspar sand and silicone putty for the brittle and ductile layers of the crust, respectively. The initial geometry of the system is a replicate of the Hellenic Thrust Wedge (see Figure2a). A rotating wall allowed the model to collapse under its own weight. Both the opening of the rotating wall (angle α) and the basal slope of the wedge (angle β; crust-mantle boundary in nature) were controlled by stepping motors. Extension was applied to the system by a constant displacement velocity. Subscripts "*i*" and "*f*" denote the initial and final values.

arecommonly considered to play an important role in back-arc extension. However, the large-scale tectonic history of the Aegean and the available geological and geophysical data (see section 2) make such a simplification acceptable (see section 3.5). To set up a modeling strategy of the gravitational collapse of a brittle-ductile wedge whose frontal boundary is submitted to a rotational extensional displacement, we took into account all available geological and geophysical data that bring constraints on the calibration of suitable initial and boundary conditions. Such conditions can be summarized as follows.

3.1.1. Initial Wedge Geometry

Extension is applied to a thrust wedge whose geometry is deduced from the restoration of extensional displacements at the scale of the Aegean (Figure 2a) [*Brun et al*., 2012). On this basis, we have chosen a mean initial wedge angle of 20° (β_i in Figure 5).

3.1.2. Topography

To take into account the topography of a crustal thickness of around 70 km at thrust wedge rear that linearly decreases frontward, we inclined the wedge surface frontward of an angle of 3° at the onset of extension.

3.1.3. Rheology

The subduction of continental blocks that rapidly undergo exhumation implies that the continental crust is delaminated from the underlying lithospheric mantle. Once delaminated, the crust comes into contact with the asthenosphere and then undergoes heating [*Brun and Faccenna*, 2008; *Tirel et al*., 2013]. This is in agreement with high-temperature metamorphism and widespread evidence of migmatization in the Rhodope core complexes [*Brun and Sokoutis*, 2007; *Burg*, 2012]. Therefore, we designed the thrust wedge at the onset of extension as dominantly ductile.

The thickness of the frictional layer that represents the upper brittle crust should depend on the thermal state of the crust, warmer at the rear than at the front as heating due to crust-mantle delamination started at the rear. To take this effect into account, the upper frictional layer was built thicker at the front. The brittle thickness was chosen as a function of the initial length of the extending domain that was around 140 km (Figure 4). Therefore, the mean thickness value of the brittle layer in our models ranges between 1.05 and 1.30 cm, corresponding in nature to the range of 7.4 to 9.1 km, respectively. Although such low values of brittle layer thickness that indicate shallow brittle-ductile transition are surprising, they are, however, in agreement with other indicators of extremely high geothermal gradients in the Aegean (e.g., heat flow

measurements as high as 100 heat flow unit). This is rather well explained by crust-mantle delamination during continental block subduction [*Brun and Faccenna*, 2008; *Tirel et al*., 2013] that brought the crustal units in direct contact with the asthenosphere, leading to fast and strong heating and widespread partial melting in the overlying crust. On top of the main body of the SRCC, there is an arc unit dated at 160 Ma [*Turpaud and Reischmann*, 2010] that was migmatized around 50 Ma, that is 5 Myr prior to the onset of core complex development. In the Chalkidiki peninsula, which is the hanging wall of the core complex detachment, the brittle-ductile transition at middle Miocene was not deeper than 10 km, as indicated by the narrow width of the Mygdonia Graben [*Kydonakis*, 2014]. Neogene basin geometry and fission track data indicate that in the SRCC, the brittle-ductile transition was in a depth range of 7–9 km soon after its exhumation [*Brun and Sokoutis*, 2014].

3.1.4. Displacements Applied at Model Boundaries

As mentioned in the introduction, Aegean extension is driven by the rollback of the Hellenic subduction. During trench retreat, the thrust wedge spreads under its own weight (i.e., gravity spreading). Restoration of displacements at the scale of the Aegean indicates that during the first 30 Myr of extension, from middle Eocene to middle Miocene, the mean velocity of trench retreat is rather constant and in the order of 0.7 cm/Myr [*Brun and Sokoutis*, 2010]. Consequently, in our models, we used a constant velocity for the displacement of the frontal boundary. Its value was calibrated as a function of the free spreading rate of the wedge at the end of the calibration run.

On the other hand, as the extensional history of the Aegean occurred during clockwise rotation (see previous section), the displacement at the wedge front in our models was accommodated by a mobile wall. A bulk angle of rotation of 30° (angle α in Figure 5) was chosen in agreement with the observed value in the SRCC [*Kondopoulou and Westphal*, 1986; *Brun and Sokoutis*, 2007]. With rotating boundary displacement like those used in our experiments, the stretching rate increases with the distance from the pole of rotation. In experiments without the rotation of the mobile wall, the stretching rate would have been constant. Comparable boundary conditions were also used by *Schellart et al*. [2003] to study back-arc deformation in northwestern Pacific. However, their brittle-ductile models have constant thickness, whereas our models are wedge shaped and aim to simulate the extension of a thrust system.

3.1.5. Variation of Wedge Angle During Extension

To control the initial wedge angle, the model was constructed on top of a rigid plate initially inclined at $\beta_i = 20°$ (Figure 5). To calibrate the decrease of wedge angle during extension, the basal plate was rotated downward at a constant rate to reach the horizontal ($\beta_f = 0°$) at the time when the chosen bulk amount of extension is attained. Because the model surface remains horizontal during the experimental run, there is no pressure gradient within the model. In other terms, the models are permanently in a quasi-isostatic equilibrium.

3.2. Scaling

The models were scaled following the principles of geometric, dynamic, kinematic, and rheological similarity [*Hubbert*, 1937; *Ramberg*, 1981]. The experimental method developed at Geosciences Rennes to study the deformation of brittle-ductile tectonic systems uses sand and silicone putty to represent brittle and ductile layers, respectively. The basic principle of the method ground on simulating simplified strength profiles that incorporate both brittle (frictional) and ductile (viscous) rheologies with gravity forces. Scaling relationships between the prototype and the model are obtained by keeping the average strength of the ductile layers correctly scaled with respect to the strength of the brittle layers and the gravity forces. Material properties and scaling parameters age given in Table 1.

In analogue experiments under normal gravity, it can be shown from the equation of dynamics [*Brun*, 1999] that

$$\sigma^* = \rho^* g L^* \tag{1}$$

where σ, ρ, g, and L are the stress, density, gravitational acceleration, and length. The asterisk denotes the model to nature ratio (e.g., $\sigma^* = \frac{\sigma_m}{\sigma_n}$). With model materials and natural rocks density being of the same order of magnitude, the equation reduces to

$$\sigma^* \approx L^* \tag{2}$$

This means that the stress ratio is roughly equal to the length ratio (i.e., thickness ratio).

Table 1. Material Properties and Scaling Parameters of Experiment MAK27[a]

Parameter		Model	Nature	Ratio
Density (brittle crust)	ρ_b (kg m^{-3})	1300	2500	0.52
Density (ductile crust)	ρ_d (kg m^{-3})	1499	2750	0.55
Gravitational acceleration	g (m s^{-2})	9.81	9.81	1
Mean thickness (brittle crust)	h_b (m)	1.3×10^{-2}	9.1×10^{3}	1.4×10^{-6}
Mean thickness (ductile crust)	h_d (m)	5.3×10^{-2}	3.7×10^{4}	1.4×10^{-6}
Velocity	(m s^{-1})	4.4×10^{-6}	1.6×10^{-10}	2.8×10^{4}
Cohesive strength	τ_c (Pa)	50	5×10^{7}	1.0×10^{-6}
Viscosity	η (Pa s)	3×10^{4}	7.6×10^{20}	4.0×10^{-17}
R_m		310	310	1.00
R_s		3.3	4.5	0.74

[a] R_m and R_s are the dimensionless Ramberg and Smoluchowski numbers, respectively. Viscosity of nature is estimated using the model to nature R_m ratio equal to unity.

The rheological-dynamic scaling of the models can be tested using nondimensional numbers given by ratios between forces acting on the models [*Ramberg*, 1981; *Sokoutis et al*., 2005]. For the brittle deformation, we consider the ratio between gravitational stress and cohesive strength:

$$R_s = \frac{\text{gravitational stress}}{\text{cohesive strength}} = \frac{\rho_b g h_b}{\tau_c} \tag{3}$$

where ρ_b, h_b, and τ_c are the density, thickness of the brittle layer, and cohesive strength, respectively (Table 1). For the viscous deformation, we consider the ratio between gravitational and viscous stresses:

$$R_m = \frac{\text{gravitational stress}}{\text{viscous stress}} = \frac{\rho_d g h_d}{\eta\,\dot{\varepsilon}} = \frac{\rho_d g h_d^2}{\eta V} \tag{4}$$

where ρ_d, h_d, η, $\dot{\varepsilon}$, and V stand for the density of the ductile layer, thickness of the ductile layer, viscosity, strain rate, and mean velocity of extension, respectively (Table 1).

Table 1 shows the comparison between the parameters of model MAK27 and their corresponding values in nature. For dynamic similarity to be fulfilled, models should share similar R_s and R_m numbers to nature. However, the respective value of mean viscosity of the ductile crust in nature (η) that is involved in equation (4) cannot be precisely known a priori. Therefore, using equation (4) and setting model to nature R_m ratio equal to unity, the estimated mean ductile crust viscosity is 7.6×10^{20} Pa s.

3.3. Materials and Strength Profiles

Dry feldspar sand was used in our models to simulate the upper brittle crust whose behavior is of Mohr-Coulomb type and follows the formulation $\tau = 50 + 0.6\sigma$, where τ and σ are the shear and normal stresses, respectively [*Byerlee*, 1978].

For frictional cohesiveness materials, the maximum (σ_1) and minimum (σ_3) principal stresses follow the Mohr-Coulomb relation:

$$\sigma_3 = \frac{1 - \sin\varphi}{1 + \sin\varphi}\sigma_1 \tag{5}$$

where φ is the angle of internal friction. In extension where the vertical stress (σ_v) is $\sigma_v = \sigma_1 = \rho g z$, the differential stress (for $\varphi = 30°$) is given by

$$\sigma_1 - \sigma_3 = \frac{2}{3}\rho g z \tag{6}$$

The above formulation is used to calculate the strength profiles for the sand layers of the model (Figure 6).

The ductile behavior of the lower crust is reproduced using a Newtonian silicone putty (Silbione: pate "gomme 70009"-Rhône Poulenc, France) with viscosity equal to 3×10^{4} Pa s measured at room temperature. The strength of the silicone layers can be calculated using the formula [*Nalpas and Brun*, 1993]:

$$\sigma_1 - \sigma_3 = 2\eta\gamma \tag{7}$$

where γ is the shear strain rate. The latter can be calculated as the ratio between the displacement velocity of the mobile wall of the model (V) and the thickness of the ductile layer (h): $\gamma = V/h$. However, this absolute

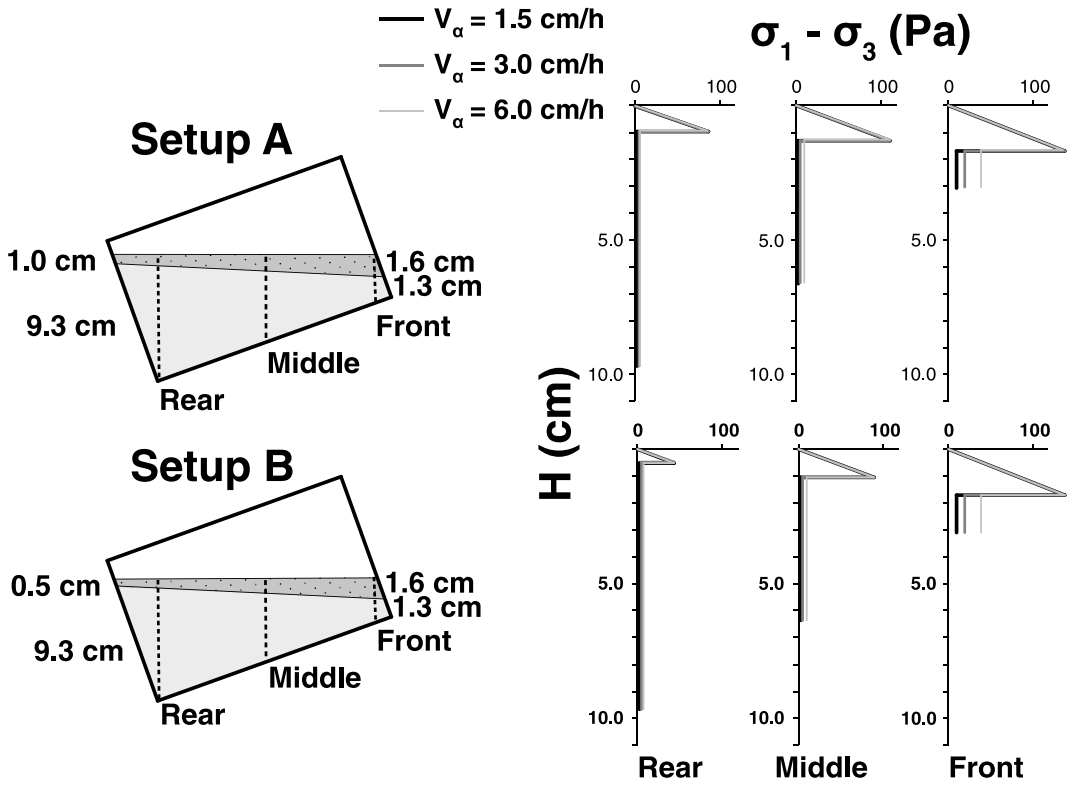

Figure 6. Model's side view and calculated strength profiles along a central transect for the two different initial geometries used in the experiments (reflecting the thickness variation in the frictional layer). Due to the variation of the sand layer thickness and displacement velocity, different strength profiles are calculated for the frontal (near the rotating wall), the middle, and the rear part (near the backstop) of the model.

value is valid only for the initiation of the each experiment, and it is anticipated to be reduced during the evolution of model deformation. As a result, for increased displacement velocity and decreased silicone putty thickness, the strength of the silicone layer exhibits that of the overlying sand layer, a case unlikely to happen in nature.

Due to the wedge-shaped initial geometry of our models (see next paragraph), three strength profiles (front, middle, and rear) have been calculated along the central transect of the model (Figure 6).

3.4. Experimental Setup

According to the modeling strategy defined in section 3.1, we set up the experiments as follows (Figure 5). Wedge-shaped sand/silicone models were constructed in a Plexiglas box (40 × 40 × 12 cm), whose walls were lubricated with liquid soap to avoid boundary effects. Models were bounded by a fixed wall at the back and a frontal rotating wall. During the model building, the Plexiglas box was inclined ($\beta_i = 20°$), and the rotating wall was set "closed" ($\alpha_i = 0°$). The base of the silicone layer corresponds to the Moho in nature. At the onset of each experiment, the model is inclined frontward by 3° to simulate a foreland-dipping surface slope.

During the experiments, the displacement of the rotating wall allowed the wedge to spread under its own weight at a constant rotation velocity (V_α) of the mobile wall that was controlled by a stepping motor. The maximum aperture α of the rotating wall, attained at the end of each experiment, was ~30°. As extension increased with increasing angle α, the basal slope β was decreased at a constant velocity V_β by another stepping motor. To fit the Aegean situation (Figure 2), V_α was locked against V_β such as $\alpha_f = 30°$ when $\beta_f = 0°$ (Figure 5).

Whereas the silicone wedge was kept the same in all experiments, two different wedge-shaped feldspar sand layers have been tested (Figure 6). The sand thickness was 1.6 cm against the mobile wall, whereas it was either 1.0 or 0.5 cm against the backstop in Setups A and B, respectively (Figure 6). The effect of the rotating wall velocity (V_α) (locked against the basal slope change—V_β) was examined.

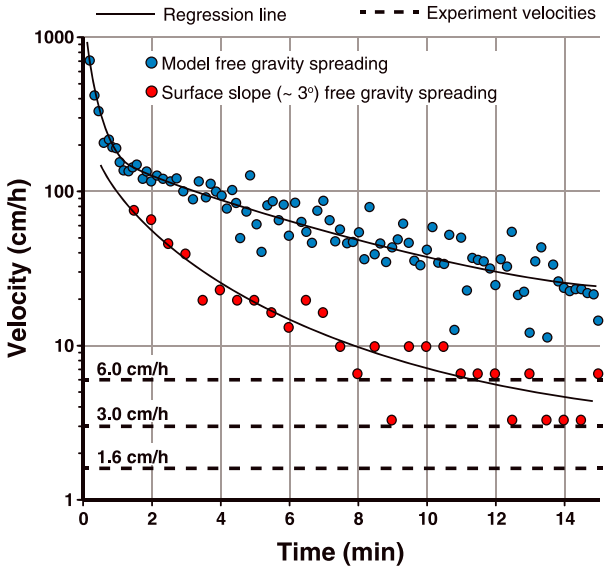

Figure 7. Variation of the spreading velocity (logarithmic scale) with time under normal gravity calibration experiments. The free gravity spreading experiments were conducted in the experimental apparatus shown in Figure 5 after the removal of the rotating wall so that the system was allowed to flow freely under the effect of gravity. The initial geometry and built of the model are described in the text. The blue and red dots represent the model front propagation velocity measured from surface photographs taken at regular time intervals. For the blue dots, the model was built as described in the text and immediately its basal slope (angle β) turned from 20° to zero, allowing the model to spread under the effect of gravity. The red dots illustrate the velocity-time curve that correspond to the smoothing of the initially imposed ~3° surface slope. During this calibration experiment, the basal slope (angle β) remained at its initial value (20°). For comparison, the three velocities used in the experiments are shown in dashed lines.

Two free-gravity spreading models have been used to calibrate the velocity values V_α and V_β: one with a 3° surface slope and one with 20° initial wedge angle (Figure 7). Velocity values of 1.6, 3.0, and 6.0 cm/h were used in the experiments and were chosen to be close to the asymptotic abscissa-parallel values of the calculated velocity-time curves of the free gravity spreading models (Figure 7).

In order to study the displacements and structure development at model surface, top-view photographs were taken at regular time intervals. For one model, we calculated a set of incremental velocity field and the corresponding surface strain rate, from pairs of top-view photographs using PIVlab updated to v.1.35 [*Thielicke and Stamhuis*, 2014]. The various geometric and kinematic parameters used in the series of experiments are summarized in Table 2.

No cross section of models is shown in the present paper as several examples of such sections were shown and discussed in previous studies [*Brun et al.*, 1994; *Brun*, 1999; *Tirel et al.*, 2006].

3.5. Model Limitations

The geometry and rheological layering of the models are necessarily simplified compared to nature. However, a simplified setting allows the first-order parameters that control the deformation pattern to be easily highlighted and understood.

Another known limitation of sand-silicone models is due to their incapacity to simulate rheological changes due to temperature variations during deformation. However, representing the lower crust by a uniform layer with depth-invariant properties has been successfully adopted in many analogue modeling experiments and is acceptable in our case study as a first-order approximation.

Analogue and numerical modeling of retreating slabs were used to demonstrate and quantify the development of toroidal mantle flow in narrow subduction systems [e.g., *Funiciello et al.*, 2003, 2006] and its role in back-arc

Table 2. Geometric and Kinematic Parameters of the Models Presented Here[a]

Model	Sand Thickness (cm) Front-Rear	Silicon Thickness (cm) Front-Rear	$V\alpha$ (cm/h)/ (deg/h)	$V\beta$ (cm/h)/ (deg/h)	Duration (h)
Setup A					
MAK27	1.6-1	1.3-9.3	(1.5) (2.5)	(2.8) (1.5)	~13
MAK25	1.6-1	1.3-9.3	(3) (5)	(5.6) (3)	~6
MAK26	1.6-1	1.3-9.3	(6) (10)	(11.2) (6)	~3
Setup B					
MAK29	1.6-0.5	1.3-9.3	(1.5) (2.5)	(2.8) (1.5)	~13
MAK28	1.6-0.5	1.3-9.3	(3) (5)	(5.6) (3)	~6
MAK30	1.6-0.5	1.3-9.3	(6) (10)	(11.2) (6)	~3

[a] $V\alpha$ is the rotating wall displacement velocity, and $V\beta$ is the wedge basal slope change velocity. Both velocities are given in cm/h and deg/h.

extension [*Duarte et al*., 2013; *Schellart and Moresi*, 2013]. However, as illustrated in the above quoted models, toroidal flow occurs when the retreating slab is laterally free. In the Aegean, lateral slab, tearing occurred at a late stage of the geodynamic history, more likely since middle Miocene, and possibly allowed toroidal flow to take place mostly in the southern part of the back-arc domain, from the Cyclades to the Hellenic trench [*Brun and Sokoutis*, 2010; *Jolivet et al*., 2013]. However, available mantle anisotropy data [*Hatzfeld et al*., 2001] do not show clear evidence of toroidal flow, even in the southern Aegean. Trench suction could also have played a role in the southern Aegean back-arc domain, close to the Hellenic trench, where dynamic topography effects can be argued [*Husson*, 2006]. The above arguments show that neglecting the effects of toroidal flow and trench suction in the present modeling work, which only concerns the northern part of the Aegean, is an acceptable simplification.

4. Experimental Results

The series of experiments presented here first aimed at testing whether an initial wedge-shaped crust geometry with a simple two-layer brittle-ductile structure is a sufficient condition to explain the first-order deformation pattern of the North Aegean domain, with respect to lower crust exhumation and without the addition of any complexity such as weak layers or other inherited discontinuities in the system, as commonly done in analogue and numerical models. To match this target, we studied the effects of two parameters on the resulting pattern: (i) the displacement velocity imposed by a rotating frontal wall and (ii) the variations of the brittle crust thickness. Setup A represented a "colder" crust with thicker sand layer, and Setup B represented a slightly "hotter" crust with reduced thickness of the sand layer (Figure 6). The two tested setups should be considered as small adjustments of an otherwise hot and thick crust and do not at all correspond to a "hot" and "cold" crust at the first place.

Selected top-view snapshots of the experiments at, almost, regular time intervals are shown in Figures 8 and 9. For convenience, the description of structures observed in top-view photographs are oriented with reference to a virtual north that is taken upward and parallel to the lateral walls of the model (see Figure 5).

4.1. Models With a Thick Brittle Layer (Setup A; Figure 8)

Three models (MAK25, MAK26, and MAK27) in which the sand layer thickness is 1.0 cm against the backstop were run with displacement velocities of 1.5, 3.0, and 6.0 cm/h at the extremity of the rotating wall (Figure 8).

At a stretching velocity of 6.0 cm/h and 25% of the bulk stretching applied to the model, a domain of faulting is located dominantly in the northeast corner of the model and along the backstop. The main fault that is almost parallel to the rotating wall curves toward the axis of rotation to the west and toward the slipping lateral boundary to the east. This main fault defines a block that rotates with the mobile wall and remains almost undeformed all along the experiment. With increasing deformation, from 25 to 100% of the bulk stretching, the northeast corner of the model is affected by conjugate and narrow spaced faults. In other words, this model is characterized by a distributed extension. At 75% of bulk stretching, a zone of silicone putty is exposed (i.e., exhumed) at the surface along the main fault that defines the undeformed rotating block.

At a stretching velocity of 1.5 cm/h, the model's behavior is strikingly different. At 25% of bulk stretching, the main faults are still propagating. At 50% of bulk stretching, they both have reached the rotation axis and have circumscribed a rotating block directly comparable to that of the model described above. Deformation is localized again to the northeast corner of the model. However, it is now localized into two faults parallel to each other at initiation. With ongoing stretching, the blocks defined by these faults separate each other progressively, allowing the silicone putty to be exhumed in between. During block separation, the borders of the northern zone of the exhumed silicone putty remained almost parallel to each other. On the contrary, the borders of the southern zone progressively formed a triangular zone of exhumation.

At a stretching velocity of 3.0 cm/h, the model behavior is intermediate, combining a zone of distributed faulting in the northeast corner of the model and along the backstop and a triangular zone of exhumation against the rotating block.

4.2. Models With a Thin Brittle Layer (Setup B; Figure 9)

Three models (MAK28, MAK29, and MAK30) in which the sand layer thickness is 0.5 cm against the backstop were run, like in the previously described models with displacement velocities of 1.5, 3.0, and 6.0 cm/h (Figure 9).

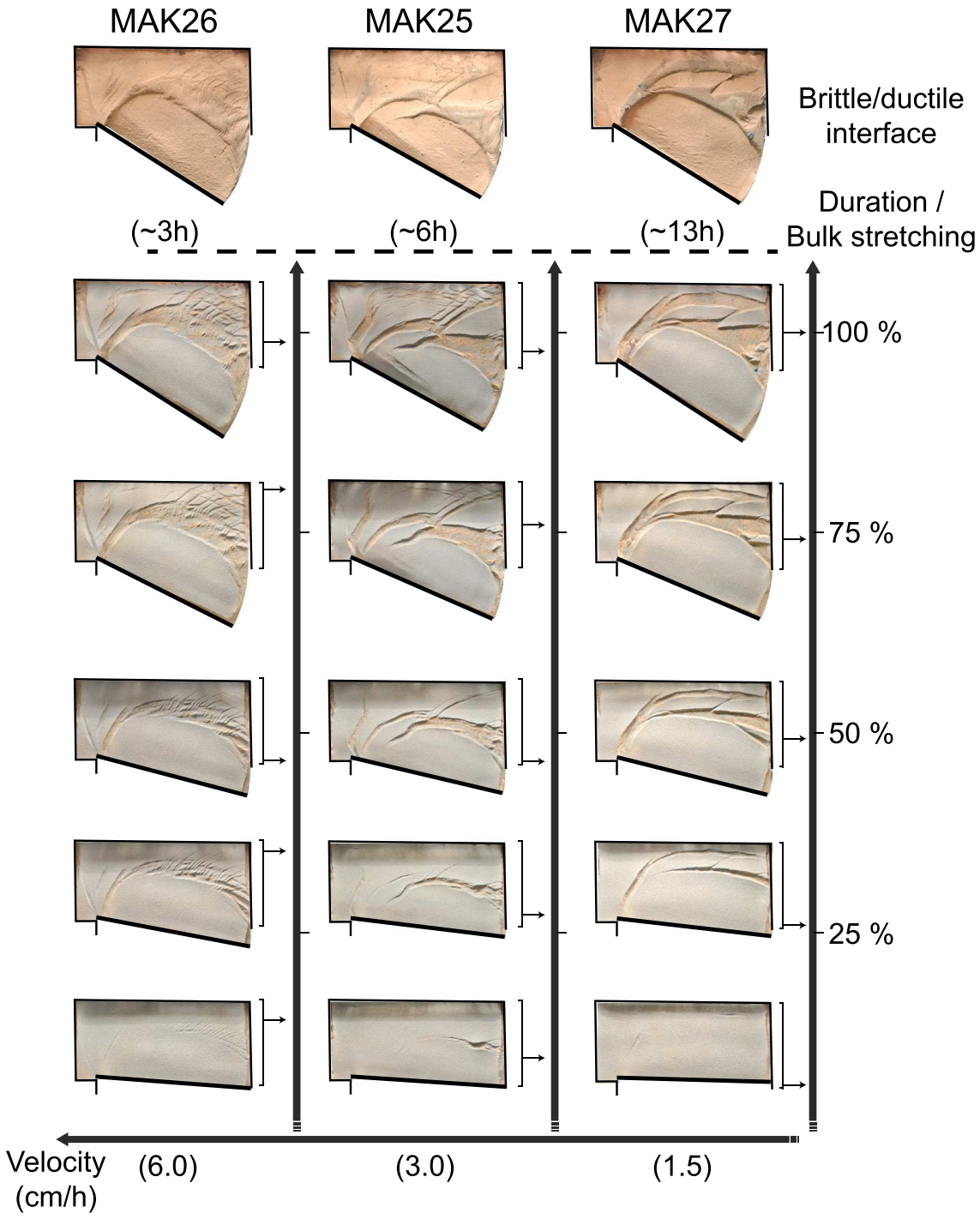

Figure 8. Selected top-view snapshots for Setup A experiments (thicker sand layer; see Figure 6) using three tested displacement velocities. The brittle-ductile interface at the end of each experiment is also shown at the top. To facilitate the discussion, a virtual north is taken as facing upward. See text for details.

These three models display a distributed deformation in the northeast corner of the model and along the backstop. With increasing stretching, velocity from 1.5 to 6.0 cm/h fault spacing decreases. It must be noted that the fault pattern of the model run at 1.5 cm/h is close to the one obtained in the previous series at a velocity of 6.0 cm/h (Figure 8). In both models, with progressive stretching a zone of silicone putty exhumation occurred along the northern border of the rotating block.

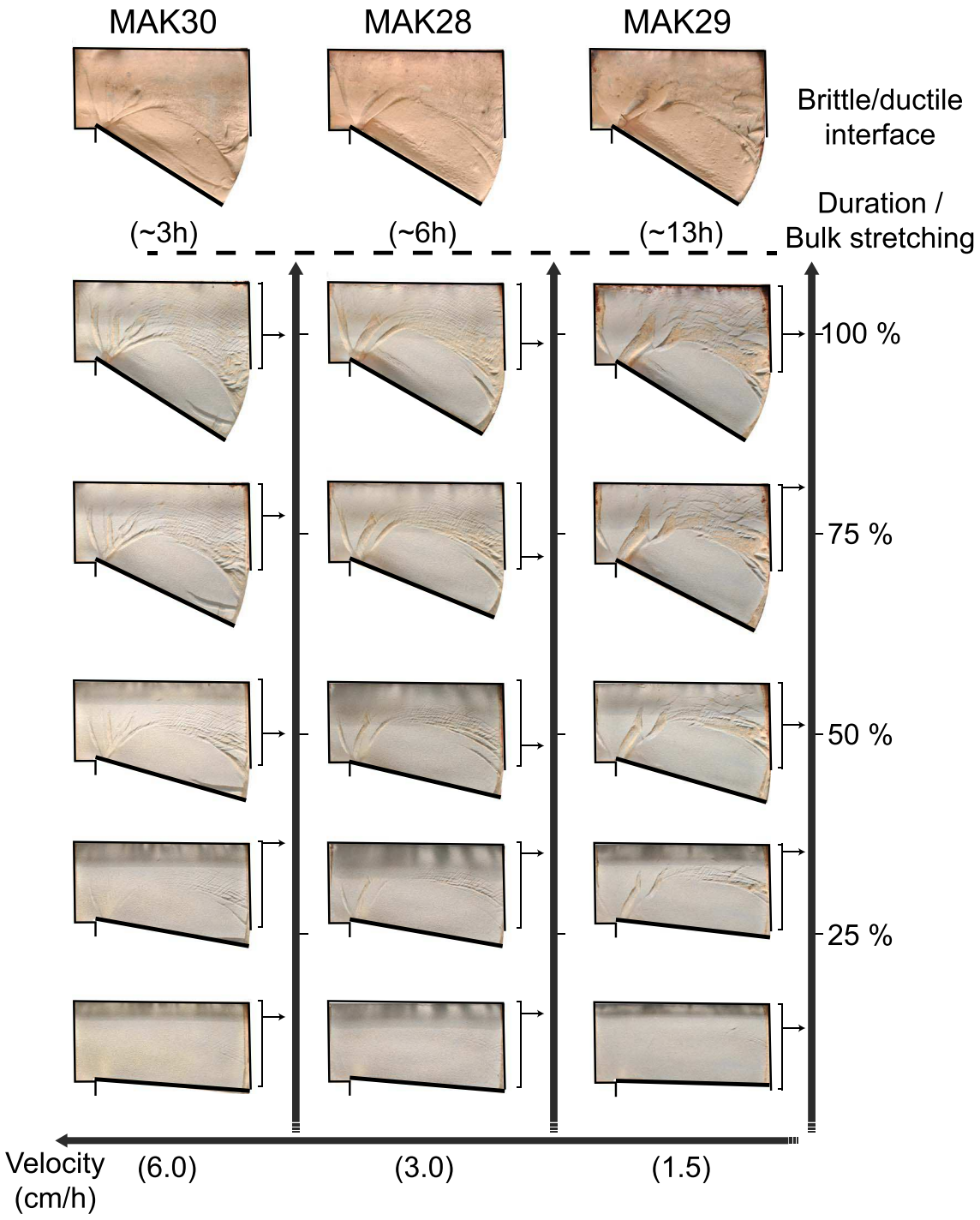

Figure 9. Selected top-view snapshots for Setup B experiments (thinner sand layer; see Figure 6) using three tested displacement velocities. The brittle-ductile interface at the end of each experiment is also shown at the top. To facilitate the discussion, a virtual north is taken as facing upward. See text for details.

5. Interpretation of the Experimental Data

5.1. Core Complex Versus Wide Rift Mode of Extension

Our experiments display either localized or distributed extension that in nature would correspond to core complex and wide rift modes of extension [see *Buck*, 1991; *Brun*, 1999], respectively (Figure 10).

The exhumation of the silicone putty starting at the onset of deformation, which is an equivalent of core complexes in nature, was obtained in two models (MAK27 and MAK25; Figure 8). One of these two models

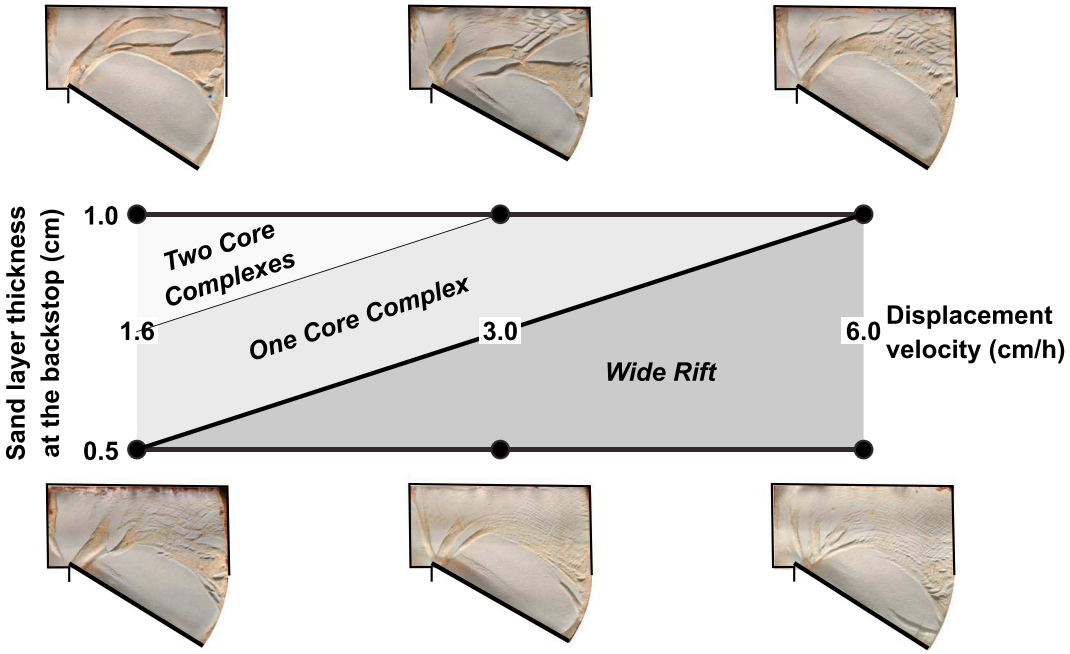

Figure 10. Compilation of the finite surface deformation pattern of the six experiments presented in this contribution (Figures 8 and 9) with respect to the resulting mode of extension. Core complex mode of extension is favored by high frictional strength (i.e., increased brittle crust thickness) and/or low ductile strength (i.e., low viscosity and low strain rate). The case where two different zones of core complex were formed (upper left corner) corresponds to the situation of the North Aegean domain discussed in the text (see also Figure 11).

(MAK27) displays two core complexes, whereas the other one (MAK25) corresponds to a mixed mode with one core complex and one wide rift zone to the north of it. The series of models (Figure 10) exemplifies that the core complex mode is favored by thick sand layer (i.e., high frictional strength) and/or low stretching rates (i.e., low ductile strength).

A wide rift mode of extension is obtained in all other models (MAK26, MAK28, MAK29, and MAK30; Figures 8 and 9). In two of these wide rift mode models (MAK26 in Figure 8 and MAK29 in Figure 9), the silicone exhumed against the rotating block after a large amount of strain (50 to 75% of bulk stretching). This exhumation pattern that is a function of strain intensity does not correspond to an initial instability of the brittle-ductile system and therefore is not representative of the core complex mode.

5.2. Progressive Development of Core Complexes

Progressive deformation in the model that displays two zones of core complexes (MAK27) is illustrated in Figure 8. Shortly after the onset of extension (~10% of the bulk stretching), deformation localized in a rear graben near the backstop. It was followed soon after ~15% of bulk stretching by a frontal graben that formed midway between the rotating wall and the backstop. Both grabens were bordered by a conjugate set of normal faults, and both opened at approximately the same rate until almost 25% of bulk stretching. Then, stretching concentrated in the frontal graben that became a zone of silicone exhumation forming, therefore, a core complex. At around 50% of bulk stretching, the frontal core complex had already exhumed silicone over a width twice as large as that of the rear graben. Silicone started to exhume in the rear graben soon after. During the second half of the experiment, the frontal core complex quadrupled its width, while the rear core complex only doubled it. Between the two core complexes, a narrow strip of undeformed material remained intact throughout the experiment. A large area, covering half the experiment's surface between the frontal core complex and the rotating wall, remained undeformed until the end of the experiment.

The velocity and surface strain rate fields of the same model MAK27 (Figure 8) were calculated using couples of successive top-view photographs and are shown in Figure 11. Three selected snapshots have been chosen to illustrate the progressive development of the core complexes. At 10% of bulk stretching, deformation occurred mostly in the rear core complex (Figure 11a). At approximately 20% of bulk stretching, the activity of

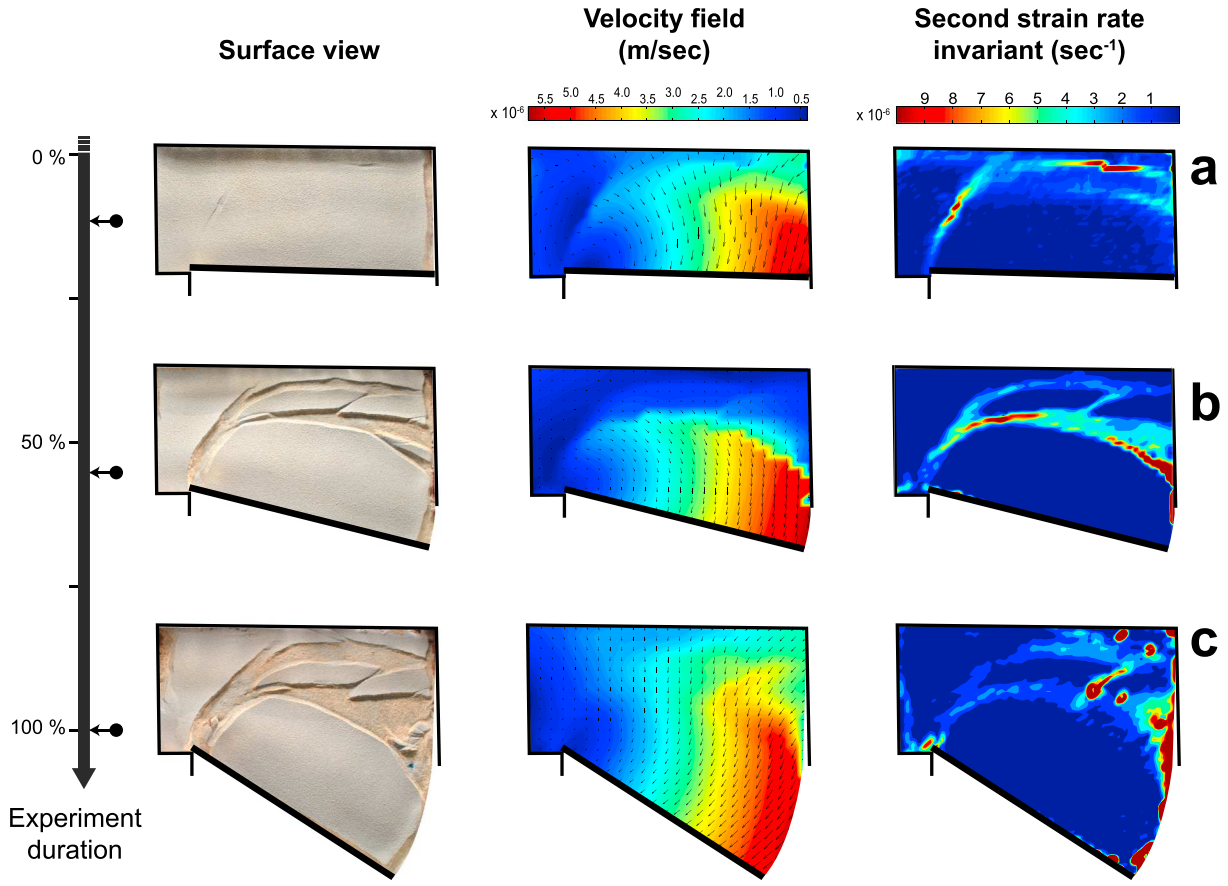

Figure 11. Selected top-view snapshots and calculated velocity field and second strain rate invariant of experiment MAK27 approximately at the (a) beginning, (b) midway, and at (c) the end of the experiment. The PIV calculations were made using PIVlab v.1.35 software (http://pivlab.blogspot.gr/). The curve-shaped pattern of the velocity field is typical for rotational driven deformation with the displacement magnitude reducing toward the pivot point. See text for details.

this rear localized; stretching strongly decreased as the frontal core complex zone initiated. Then up to 60% of bulk stretching, the strain localized in the frontal core complex with the maximum strain rate values located against the undeformed rotating block (Figure 11b). In nature, this high-strain rate zone would correspond to the extensional detachment zone that controls core complex exhumation. It is noteworthy that between 30 and 60% of bulk stretching, the detachment zone remained located against the undeformed rotating block. After 60% and up to 100% of bulk stretching, strain tend to localize in the largely widening part of the core complex, to the east close to the curved lateral boundary, and along strike-slip shear zones that cut through the block that separate the two core complexes (Figure 11c).

5.3. Location of Stretching at the Wedge Rear

All models have in common: (i) the isolation by faulting of a block against the rotating wall that remained undeformed during the whole experiment and (ii) the deformation that localized in the northeast corner and along the backstop, either appearing with a localized or a distributed pattern (Figures 8 and 9).

With increasing extension, the wedge angle β decreases progressively down to horizontal at the end of the experiment. At wedge back, the bulk vertical shortening is $\lambda_v = t_f/t_b$, where t_b is the initial thickness at wedge back and t_f is the constant model thickness at the end of experiment. Assuming plane strain in the direction perpendicular to the backstop $\lambda_h\,\lambda_v = 1$, where λ_h is the bulk horizontal stretching. Therefore, the bulk horizontal stretching is $\lambda_h = t_b/t_f$, which for $t_f = 2.9$ cm and $t_b = 9.8$ cm (see Figure 6) gives $\lambda_h = 3.4$. This shows that stretching at wedge rear is higher than 200%. Stretching at the front, against the mobile wall is essentially zero because the frontal part of the model corresponds to the rotating and nondeforming block.

As a result, stretching is strongly concentrated in the back part of the wedge. In other terms, the localization of stretching at model's rear is a direct consequence of the initial wedge shape of the deforming system.

6. Discussion

The set of laboratory experiments presented in this paper has two types of outcomes: first, on a general ground, those concerning core complex development as a result of extension of a thrust wedge and second, those related to application to natural extensional systems and in particular to back-arc extension in the North Aegean domain.

6.1. Core Complex Development in a Thrust Wedge Undergoing Gravity Spreading

6.1.1. Stretching Located at the Wedge Rear

Previous models of core complex extension, either analogue [e.g., *Brun et al*., 1994; *Tirel et al*., 2006] or numerical [e.g., *Tirel et al*., 2004a, 2008; *Wijns et al*., 2005; *Rey et al*., 2009a, 2009b], considered a brittle-ductile crust with an initial constant thickness. Such an initial geometry requires some type of rheological weakness to be introduced in the model to boost strain localization during early stages of extension. Such a weakness could either be (i) a preexisting fault in the upper brittle crust [e.g., *Koyi and Skelton*, 2001; *Gessner et al*., 2007; *Rey et al*., 2009a, 2009b] or (ii) a local heterogeneity below the brittle-ductile transition (weaker than the surrounding ductile layer) [e.g., *Brun et al*., 1994; *Tirel et al*., 2004a, 2008]. However, few models involving strain-dependent fault weakening [e.g., *Regenauer-Lieb et al*., 2006; *Tirel et al*., 2009] have been able to stimulate core complex development without the presence of inherited weaknesses.

As demonstrated in our models, contrary to what has been discussed at length for core complex development in a constant thickness brittle-ductile crust, no inherited weak zone (brittle or ductile) or particular mechanism of rheological weakening is required to stimulate the strain localization and core complex formation in an extending wedge-shaped system. In such common thrust wedges submitted to extension, the only necessary condition for core complex development is the presence of a thick and low-strength (i.e., weak) ductile crust.

During the gravity spreading of thrust wedges, the horizontal stretching directly depends on the initial layer thickness, and thus, stretching intensity increases toward the rear of the extending system where thickness is increased. In other words, localization of core complex extension at wedge rear is intrinsically related to the wedge shape of the extending system.

6.1.2. Location and Dip of the Detachment

As illustrated in our models, the extending domain located at wedge rear is separated from the mobile boundary by a nonextending and only translating block that corresponds to the thin frontal part of the wedge. During the core complex exhumation, strain remains localized against this undeforming block (Figure 11). This high-strain zone corresponds to the detachment of the core complex. In other words, in an extending brittle-ductile wedge, the detachment that controls core complex exhumation is located against and dips toward the nonextending thin frontal part of the wedge.

6.2. Core Complex Development in the North Aegean

6.2.1. North Aegean Core Complexes

As summarized in section 2, the Hellenic Thrust Wedge is the result of successive closure of the Vardar and Pindos oceanic domains and the piling up of Rhodopia, Pelagonia, and External Hellenides that assembled by Eocene (Figures 1 and 2a). In Eocene, the thrust wedge was submitted to extension, controlled by the onset of the Hellenic slab rollback (Figures 2a and 2b). This led to the formation of partly migmatized core complexes to the North Aegean that are (i) the aligned extensional metamorphic domes (Chepinska, Arda, Kardamos-Kesebir, and Kechros-Biela-Reka) to the northeast [see *Burg*, 2012] and (ii) the larger Southern Rhodope Core Complex (SRCC) to the southwest [*Brun and Sokoutis*, 2007] (Figure 3). The first domes (called here for convenience as the "Northern Rhodope Core Complex" (NRCC)) developed within the Northern Rhodope Domain, whereas the latter separated Rhodopia into two main blocks: the Northern Rhodope Domain and the Chalkidiki block to the northeast and southwest, respectively (Figures 1 and 3).

The exhumation of the SRCC was controlled by the Kerdylion Detachment, whose hanging wall (the Chalkidiki block) remained almost undeformed for ~30 Myr (from middle Eocene to middle Miocene) until the formation of the Mygdonia basin [*Koufos et al*., 1995]. During the exhumation of the SRCC, the Chalkidiki block underwent an ~30° clockwise rotation facilitating its exhumation [*Kondopoulou and*

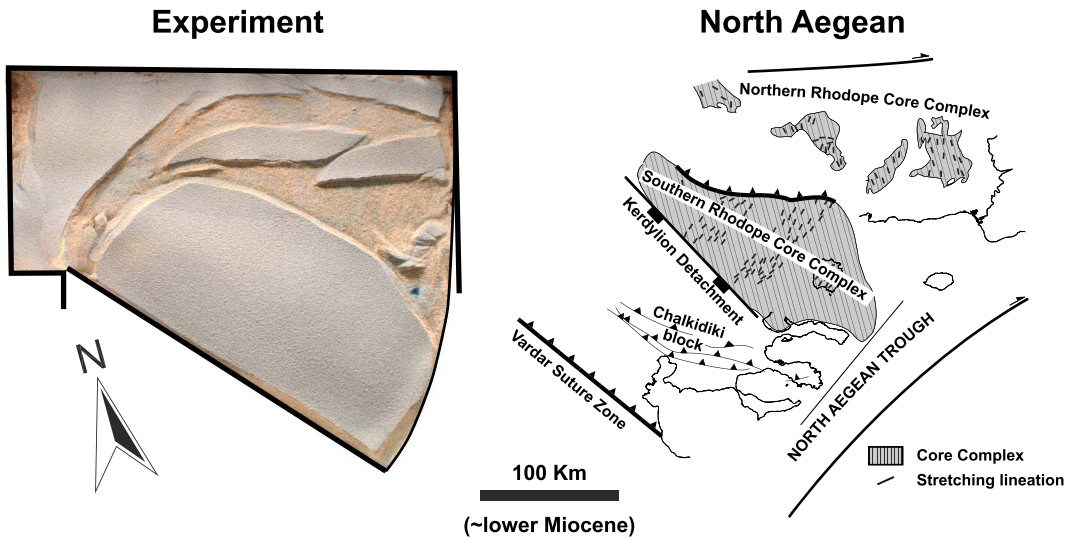

Figure 12. On-scale comparison between model results (MAK27) and the restored geometry of the North Aegean at lower Miocene with respect to core complex formation. The striking similarities between nature and model in terms of location, size, and shape of lower crust (silicone putty) exhumation are marked. The existence of a virtually undeformed block near the rotating wall that corresponds directly to the Chalkidiki block in nature is also marked.

Westphal, 1986]. Based on the deposition age of sediments and/or volcanic activity centers that developed on the metamorphics, a southwestward migration of the extension from Paleogene to Neogene can be inferred (Figure 4).

6.2.2. Comparison With Models

The wedge geometry of our models was designed on the basis of our reconstruction of the Hellenic Thrust Wedge (Figure 2a). To take into account the kinematics of extension in the North Aegean (30° clockwise rotation of the Chalkidiki block), the mobile boundary that allowed the model to spread under its own weight was pulled in rotation around a vertical axis (compare Figure 4 to Figure 5). Model rheology took into account the widespread evidence of partial melting within the NRCC and SRCC, indicating that the thrust wedge at the onset of extension was likely dominantly ductile. As the information on the initial brittle crust is very poor, we tested different geometries for the upper brittle crust. As the strength of a viscous material depends not only on its viscosity but also on the strain rate, we tested a range of extension velocities. The latter were applied at the mobile boundary (Figure 5) and were calibrated against the free spreading of the brittle-ductile wedge model (Figure 7). In our experiments, the system stretched approximately 20 cm (140 km in nature) for a period that corresponds to nature to roughly 30 Myr. This equals to a spreading rate of ~0.5 cm/yr, compatible with the estimated value from field observations for the same time span ("significantly less than 1.0 cm/yr" according to *Brun and Sokoutis* [2010]).

This experimental strategy provided a series of models that displayed two main types of extensional patterns: Wide rift versus core complex (Figure 10). Whatever the applied extension rate, in all our experiments, the deformation concentrated to the rearmost half of the box, leaving an undeformed block adjacent to the rotating wall.

The model MAK27 fairly reproduces the main extensional geological features of the North Aegean domain from middle Eocene to middle Miocene (i.e., from 45 to 15 Ma) (Figure 12), prior to the distributed extension that controlled the deposition of Neogene sedimentary basins over the whole Aegean domain (Figure 4c). The model displays (i) two core complex zones (rear and frontal) located to the north of the extending domain that directly compare with the Northern (NRCC) and Southern (SRCC) Rhodope Core Complexes and (ii) an undeformed rotated block that directly compares to the Chalkidiki block (Figure 12). In addition, the mapping of strain rate at the model's surface shows that the detachment that controlled the frontal core complex is located against the undeformed rotated block (Figure 11b) that directly compares with the Kerdylion Detachment (Figure 12). The fairly good similarities between our model and the North Aegean domain in terms of timing, location, shape, and size of the core complexes are striking, in spite of the gross

simplifications of the model. This validates the restored Eocene geometry of the Hellenic Thrust Wedge (used to design the initial geometry of our models; Figure 2). The model demonstrates that it is the initial wedge geometry of the system and the hot and thick nature of the crust (dominantly ductile) at the onset of extension that controlled the first-order deformation pattern of the North Aegean domain and especially the development of core complexes.

Whereas data on the pre-Neogene tectonic story of the North Aegean Through are lacking, the good fit between our model and the North Aegean geology (Figure 12) also suggests that the North Aegean Through that is the most prominent of the North Aegean Sea is inherited from the early Cenozoic tectonic history and that more likely it represents a major transfer zone that accommodated the rotation of the Chalkidiki block and the exhumation of the Rhodopean core complexes. It is noteworthy that the North Aegean Through falls in line with the limit between the Rhodope core complexes, in which deep hot crust exhumed in Eocene and the Thrace Basin that was a marine sedimentary basin in the same period (Figure 1). This strong contrast of extension style on the two sides of the North Aegean Through suggests that the crust was not strongly thickened to the Eastern side, allowing seawater to invade the extending domain.

7. Conclusions

The set of laboratory experiments presented here aimed at testing the gravity spreading of a trust wedge as a suitable process for the development of core complexes with particular application to North Aegean extension, during the early evolution of the Hellenic rollback. Beyond their specific application to the North Aegean, our experiments have general outcomes that potentially apply to all tectonic settings when a thrust wedge undergoes extension. They are especially appropriate to the analysis of back-arc extension driven by slab rollback [e.g., *Royden*, 1993; *Brun and Faccenna*, 2008; *Tirel et al*., 2013] as well as to eduction in which a previously subducted continental lithosphere is subsequently exhumed by subduction inversion [e.g., *Andersen et al*., 1991; *Mishin et al*., 2008; *Duretz et al*., 2012].

7.1. Extension of a Thrust Wedge Undergoing Gravity Spreading

On a general ground, our main results can be summarized as follows:

1. Extension, either being distributed (wide rift) or localized (core complex), is located at wedge rear because in gravity spreading, the horizontal stretching depends directly on the thickness of the material that is subject to spreading. Thus, the wedge rear being thicker than the frontal part undergoes stronger stretching.
2. The core complex detachment is located against and dips toward the nonextending thin frontal part of the wedge.
3. Core complex location as well as detachment location and dip are interdependent and intrinsically related to the initial wedge shape of the extending system.
4. The experiments presented here show that the development of core complexes is favored (i) by high frictional strength (i.e., increased brittle crust thickness) and/or (ii) by low ductile strength (i.e., low viscosity and low strain rate). Therefore, a partially molten crust (very low viscosity) that is slowly stretched is an ideal candidate to undergo core complex mode of extension. We note that this conclusion applies to all core complexes and not only to those developed in a spreading wedge. As already stated in previous studies [e.g., *Tirel et al*., 2008; *Whitney et al*., 2013], core complex development is favored by thick and weak ductile crust.

7.2. Extension of the North Aegean Domain

Similarities between structures that developed in our model and those of the North Aegean domain are striking in spite of the simplifications inherent to modeling (Figure 12).

1. *Location*: Two core complexes initiated in the back part of the wedge and are separated from the wedge front by an undeformed block.
2. *Sequence of development*: Extension started close to the wedge backstop (rear core complex/Northern Rhodope Core Complex) and rapidly migrated southward (frontal core complex/Southern Rhodope Core Complex).
3. *Size*: The rear core complex and the Northern Rhodope Core Complex remained smaller (they were likely aborted), whereas the frontal core complex and Southern Rhodope Core Complex constantly enlarged since their initial formation.

4. *Detachment*: Exhumation in both the frontal core complex and the Southern Rhodope Core Complex was controlled by a detachment located against and dipping toward the frontal undeformed block that is direct equivalent to the Chalkidiki block in nature.
5. *Shape*: The rear core complex and the Northern Rhodope Core Complex remained almost parallel to the backstop, whereas the frontal core complex and the Southern Rhodope Core Complex acquired a triangular shape as the detachment's hanging wall block rotated clockwise during stretching.

The model strengthens, that it is, the initial wedge geometry of the system and the hot and thick nature of the crust at the onset of extension that controlled the extensional pattern of the North Aegean domain and, in particular, the development of core complexes at the rear of the thrust wedge since the early stages of slab rollback.

Acknowledgments
This work was funded by the European Union FP7 Marie Curie ITN "TOPOMOD" contract 264517. D. Sokoutis acknowledge the financial support received from the Netherlands Research Centre for Integrated Solid Earth Science. We wish to thank J.-J. Kermarrec for his help in the conception and design of the experimental setting used for our experiments. We thank Benjamin Guillaume and Evangelos Moulas for their invaluable help with the PIVLab MATLAB script used for the calculations of the velocity/strain fields shown in Figure 11. We thank Jean-Pierre Burg for the discussions on the kinematics of the southern Bulgaria core complexes. Editorial handling by Paul Tregoning as well as comprehensive reviews by João Duarte and an anonymous reviewer are greatly acknowledged. Data presented in this contribution are available upon request to K.K. (konstantinos.kydonakis@gmail.com).

References

Andersen, T. B., B. Jamtveit, J. F. Dewey, and E. Swensson (1991), Subduction and eduction of continental crust: Major mechanisms during continent-continent collision and orogenic extensional collapse, a model based on the south Norwegian Caledonides, *Terra*, *3*(3), 303–310, doi:10.1111/j.1365-3121.1991.tb00148.x.

Bijwaard, H., W. Spakman, and E. R. Engdahl (1998), Closing the gap between regional and global travel time tomography, *J. Geophys. Res.*, *103*(B12), 30,055–30,078, doi:10.1029/98JB02467.

Brun, J.-P. (1999), Narrow rifts versus wide rifts: Inferences for the mechanics of rifting from laboratory experiments, *Philos. Trans. R. Soc. London, Ser. A*, *A357*, 695–710.

Brun, J.-P., and C. Faccenna (2008), Exhumation of high-pressure rocks driven by slab rollback, *Earth Planet. Sci. Lett.*, *272*, 1–7, doi:10.1016/j.epsl.2008.02.038.

Brun, J.-P., and D. Sokoutis (2007), Kinematics of the Southern Rhodope Core Complex (north Greece), *Int. J. Earth Sci. (Geol. Rundsch.)*, *96*, 1079–1099, doi:10.1007/s00531-007-0174-2.

Brun, J.-P., and D. Sokoutis (2010), 45 Myr of Aegean crust and mantle flow driven by trench retreat, *Geology*, *38*, 815–818, doi:10.1130/G30950.1.

Brun, J.-P., and D. Sokoutis (2014), Development of ramp-flat structures during Aegean extension, *Geophys. Res. Abstr.*, *16*, EGU2014–7649.

Brun, J.-P., and J. van den Driessche (1994), Extensional gneiss domes and detachment fault systems: Structure and kinematics, *Bull. Soc. Geol. Fr.*, *165*(6), 519–530.

Brun, J.-P., D. Sokoutis, and J. van den Driessche (1994), Analogue modeling of detachment fault systems and core complexes, *Geology*, *22*(4), 319–322, doi:10.1130/0091-7613(1994)022<0319:AMODFS>2.3.CO;2.

Brun, J.-P., C. Tirel, M. Philippon, E. Burov, C. Faccenna, F. Gueydan, and S. Lebedev (2012), On the role of horizontal displacements in the exhumation of high pressure metamorphic rocks, *Geophys. Res. Abstr.*, *14* EGU2012–9381.

Buck, W. R. (1991), Modes of continental lithospheric extension, *J. Geophys. Res.*, *96*(B12), 20,161–20,178, doi:10.1029/91JB01485.

Burchfiel, B. C., R. Nakov, N. Dumurdzanov, D. Papanikolaou, T. Tzankov, T. Serafimovski, R. W. King, V. Kotzev, A. Todosov, and B. Nurce (2008), Evolution and dynamics of the Cenozoic tectonics of the South Balkan extensional system, *Geosphere*, *4*, 919–938, doi:10.1130/GES00169.1.

Burg, J.-P. (2012), Rhodope: From Mesozoic convergence to Cenozoic extension. Review of petro-structural data in the geochronological frame, *J. Virtual Explor.*, *42*, doi:10.3809/jvirtex.2011.00270.

Burg, J.-P., Z. Ivanov, L.-E. Ricou, D. Dimov, and L. Klain (1990), Implications of shear-sense criteria for the tectonics evolution of the Central Rhodope massif, southern Bulgaria, *Geology*, *18*, 451–454, doi:10.1130/0091-7613(1990)018.

Burg, J.-P., I. Godfriaux, and L.-E. Ricou (1995), Extension of the Mesozoic Rhodope thrust units in the Vertiskos-Kerdilion Massifs, *C. R. Acad. Sci. Paris*, *320*(IIa), 889–896.

Burg, J.-P., L.-E. Ricou, Z. Ivanov, I. Godfriaux, D. Dimov, and L. Klain (1996), Syn-metamorphic nappe complex in the Rhodope Massif Structure and kinematics, *Terra Nova*, *8*(1), 6–15, doi:10.1111/j.1365-3121.1996.tb00720.x.

Byerlee, J. (1978), Friction of rocks, *Pure Appl. Geophys.*, *116*(4–5), 615–626, doi:10.1007/BF00876528.

Coney, P. J. (1980), Cordilleran Metamorphic Core Complexes: An overview, *Geol. Soc. Am. Mem.*, *153*, 7–31, doi:10.1130/MEM153-p7.

Conrad, C. P., and C. Lithgow-Bertelloni (2002), How mantle slabs drive plate tectonics, *Science*, *298*(5591), 207–209, doi:10.1126/science.1074161.

Cosca, M. A., E. J. Essene, K. Mezger, and B. A. van der Pluijm (1995), Constraints on the duration of tectonic processes: Protracted extension and deep-crustal rotation in the Grenville orogen, *Geology*, *23*(4), 361–364, doi:10.1130/0091-7613(1995)023<0361:COTDOT>2.3.CO;2.

Crittenden, M., J. Peter, and C. G. H. Davis (1980), Cordilleran Metamorphic Core Complexes, *Geol. Soc. Am. Mem.*, *153*, 1–490.

Davis, G. H., and P. J. Coney (1979), Geologic development of the cordilleran metamorphic core complexes, *Geology*, *7*(3), 120–124.

Dercourt, J., L. E. Ricou, and B. Vrielynck (1993), *Atlas Tethys palaeoenvironmental maps*, Gauthier-Villars, Paris.

Dewey, J., and C. Sengör (1979), Aegean and surrounding regions: Complex multiplate and continuum tectonics in a convergent zone, *Geol. Soc. Am. Bull.*, *90*, 84–92, doi:10.1130/0016-7606(1979)90<84:AASRCM>2.0.CO;2.

Dewey, J. F. (1988), Extensional collapse of orogens, *Tectonics*, *7*(6), 1123–1139, doi:10.1029/TC007i006p01123.

Duarte, J. C., W. P. Schellart, and A. R. Cruden (2013), Three-dimensional dynamic laboratory models of subduction with an overriding plate and variable interplate rheology, *Geophys. J. Int.*, *195*, 47–66, doi:10.1093/gji/ggt257.

Duretz, T., T. V. Gerya, B. J. P. Kaus, and T. B. Andersen (2012), Thermomechanical modeling of slab eduction, *J. Geophys. Res.*, *117*, doi:10.1029/2012JB009137.

Dyksterhuis, S., P. Rey, R. Müller, and L. Moresi (2007), Effects of initial weakness on rift architecture, *Geol. Soc. Spec. Publ.*, *282*, 443–455, doi:10.1144/SP282.18.

Funiciello, F., C. Faccenna, D. Giardini, and K. Regenauer-Lieb (2003), Dynamics of retreating slabs: 2. Insights from three-dimensional laboratory experiments, *J. Geophys. Res.*, *108*(B4), doi:10.1029/2001JB000896.

Funiciello, F., M. Moroni, C. Piromallo, C. Faccenna, A. Cenedese, and H. A. Bui (2006), Mapping mantle flow during retreating subduction: Laboratory models analyzed by feature tracking, *J. Geophys. Res.*, *111*, doi:10.1029/2005JB003792.

Gautier, P., and J.-P. Brun (1994), Crustal-scale geometry and kinematics of late-orogenic extension in the central Aegean (Cyclades and Evvia Island), *Tectonophysics*, *238*(1–4), 399–424, doi:10.1016/0040-1951(94)90066-3.

Gautier, P., J.-P. Brun, and L. Jolivet (1993), Structure and kinematics of Upper Cenozoic extensional detachment on Naxos and Paros (Cyclades Islands, Greece), *Tectonics*, *12*(5), 1180–1194, doi:10.1029/93TC01131.

Gessner, K., C. Wijns, and L. Moresi (2007), Significance of strain localization in the lower crust for structural evolution and thermal history of metamorphic core complexes, *Tectonics*, *26*, doi:10.1029/2004TC001768.

Hatzfeld, D., E. Karagianni, I. Kassaras, A. Kiratzi, E. Louvari, H. Lyon-Caen, K. Makropoulos, P. Papadimitriou, G. Bock, and K. Priestley (2001), Shear wave anisotropy in the upper mantle beneath the Aegean related to internal deformation, *J. Geophys. Res.*, *106*(B12), 30,737–30,753, doi:10.1029/2001JB000387.

Hubbert, K. M. (1937), Theory of scale models as applied to the study of geologic structures, *Geol. Soc. Am. Bull.*, *48*, 1459–1519.

Huet, B., L. le Pourhiet, L. Labrousse, E. Burov, and L. Jolivet (2011a), Post-orogenic extension and metamorphic core complexes in a heterogeneous crust: The role of crustal layering inherited from collision. Application to the Cyclades (Aegean domain), *Geophys. J. Int.*, *184*, 611–625, doi:10.1111/j.1365-246X.2010.04849.x.

Huet, B., L. le Pourhiet, L. Labrousse, E. Burov, and L. Jolivet (2011b), Formation of metamorphic core complex in inherited wedges: A thermomechanical modelling study, *Earth Planet. Sci. Lett.*, *309*, 249–257, doi:10.1016/j.epsl.2011.07.004.

Husson, L. (2006), Dynamic topography above retreating subduction zones, *Geology*, *34*, 741–744, doi:10.1130/G22436.1.

Jolivet, L., and J.-P. Brun (2010), Cenozoic geodynamic evolution of the Aegean, *Int. J. Earth Sci. (Geol. Rundsch.)*, *99*, 109–138, doi:10.1007/s00531-008-0366-4.

Jolivet, L., and C. Faccenna (2000), Mediterranean extension and the Africa-Eurasia collision, *Tectonics*, *19*(6), 1095–1106, doi:10.1029/2000TC900018.

Jolivet, L., E. Lecomte, B. Huet, Y. Denèle, O. Lacombe, L. Labrousse, L. le Pourhiet, and C. Mehl (2010), The North cycladic detachment system, *Earth Planet. Sci. Lett.*, *289*, 87–104, doi:10.1016/j.epsl.2009.10.032.

Jolivet, L., et al. (2013), Aegean tectonics: Strain localisation, slab tearing and trench retreat, *Tectonophysics*, *597–598*, 1–33, doi:10.1016/j.tecto.2012.06.011.

Karson, J. (1990), Seafloor spreading on the Mid-Atlantic Ridge: Implications for the structure of ophiolites and oceanic lithosphere produced in slow-spreading environments, in *Ophiolites: Oceanic Crustal Analogues: Proc. Symp. "Troodos 1987": Nicosia*, edited by J. Malpas et al., pp. 547–555, Geol. Surv. Dep., Nicosia.

Kissel, C., and C. Laj (1988), The tertiary geodynamical evolution of the Aegean arc: A paleomagnetic reconstruction, *Tectonophysics*, *146*(1–4), 183–201, doi:10.1016/0040-1951(88)90090-X.

Kondopoulou, D., and M. Westphal (1986), Paleomagnetism of the tertiary intrusives from Chalkidiki (northern Greece), *J. Geophys.*, *59*, 62–66.

Koufos, G. D., G. E. Syrides, D. S. Kostopoulos, and K. K. Koliadimou (1995), Preliminary results about the stratigraphy and the palaeoenvironment of Mygdonia basin Macedonia, Greece, *Geobios*, *18*, 243–249.

Koyi, H. A., and A. Skelton (2001), Centrifuge modelling of the evolution of low-angle detachment faults from high-angle normal faults, *J. Struct. Geol.*, *23*(8), 1179–1185, doi:10.1016/S0191-8141(00)00185-1.

Kydonakis, K. (2014), Mesozoic Tectonics of the Aegean, PhD thesis, Géosciences Rennes.

Le Pichon, X., and J. Angelier (1979), The hellenic arc and trench system: A key to the neotectonic evolution of the eastern Mediterranean area, *Tectonophysics*, *60*(1–2), 1–42, doi:10.1016/0040-1951(79)90131-8.

Le Pichon, X., and J. Angelier (1981), The Aegean sea, *Philos. Trans. R. Soc. London, Ser. A*, *300*, 357–372.

McKenzie, D. (1978), Active tectonics of the Alpine-Himalayan belt: The Aegean Sea and surrounding regions, *Geophys. J. Int.*, *55*(1), 217–265, doi:10.1111/j.1365-246X.1978.tb04759.x.

Mercier, J. (1981), Extensional-compressional tectonics associated with the Aegean arc: Comparison with the Andean Cordillera of south Peru - north Bolivia, *Philos. Trans. R. Soc. London, Ser. A*, *300*, 337–355.

Mercier, J., N. Delibassis, A. Gauthier, J. Jarrige, F. Lemeille, H. Philip, M. Sebrier, and D. Sorel (1979), La neotectonique de l'arc Egèen, *Rev. Geol. Dyn. Geogr. Phys.*, *21*, 67–92.

Mishin, Y. A., T. V. Gerya, J.-P. Burg, and J. A. Connolly (2008), Dynamics of double subduction: Numerical modeling, *Phys. Earth Planet. Inter.*, *171*, 280–295.

Nalpas, T., and J.-P. Brun (1993), Salt flow and diapirism related to extension at crustal scale, *Tectonophysics*, *288*(3–4), 349–362, doi:10.1016/0040-1951(93)90348-N.

Norton, M. (1986), Late Caledonide Extension in western Norway: A response to extreme crustal thickening, *Tectonics*, *5*(2), 195–204, doi:10.1029/TC005i002p00195.

Papanikolaou, D. (2009), Timing of tectonic emplacement of the ophiolites and terrane paleogeography in the Hellenides, *Lithos*, *108*, 262–280, doi:10.1016/j.lithos.2008.08.003.

Papanikolaou, D. J. (2013), Tectonostratigraphic models of the Alpine terranes and subduction history of the Hellenides, *Tectonophysics*, *595–596*, 1–24, doi:10.1016/j.tecto.2012.08.008.

Philippon, M., J.-P. Brun, and F. Gueydan (2012), Deciphering subduction from exhumation in the segmented Cycladic Blueschist Unit (Central Aegean, Greece), *Tectonophysics*, *524–525*, 116–134, doi:10.1016/j.tecto.2011.12.025.

Ramberg, H. (1981), *Gravity, Deformation, And The Earth's Crust: In Theory, Experiments, And Geological Applications*, 2nd revised ed., Academic Press Inc., London.

Regenauer-Lieb, K., R. F. Weinberg, and G. Rosenbaum (2006), The effect of energy feedbacks on continental strength, *Nature*, *442*, 67–70, doi:10.1038/nature04868.

Rey, P., C. Teyssier, and D. Whitney (2009a), Extension rates, crustal melting, and core complex dynamics, *Geology*, *37*, 391–394, doi:10.1130/G25460A.1.

Rey, P., C. Teyssier, and D. Whitney (2009b), The role of partial melting and extensional strain rates in the development of metamorphic core complexes, *Tectonophysics*, *477*, 135–144.

Ricou, L.-E., J.-P. Burg, I. Godfriaux, and Z. Ivanov (1998), Rhodope and Vardar: The metamorphic and the olistostromic paired belts related to the Cretaceous subduction under Europe, *Geodinamica Acta*, *11*(6), 285–309.

Ring, U., J. Glodny, T. Will, and S. Thomson (2010), The hellenic subduction system: High-pressure metamorphism exhumation, normal faulting, and large-scale extension, *Annu. Rev. Earth Planet. Sci.*, *38*, 45–76, doi:10.1146/annurev.earth.050708.170910.

Robertson, A. H. (2002), Overview of the genesis and emplacement of Mesozoic ophiolites in the Eastern Mediterranean Tethyan region, *Lithos*, *65*(1–2), 1–67, doi:10.1016/S0024-4937(02)00160-3.

Royden, L. H. (1993), Evolution of retreating subduction boundaries formed during continental collision, *Tectonics*, *12*(3), 629–638, doi:10.1029/92TC02641.

Royden, L. H., and D. J. Papanikolaou (2011), Slab segmentation and late Cenozoic disruption of the Hellenic arc, *Geochem., Geophys., Geosyst.*, *12*, Q03010, doi:10.1029/2010GC003280.

Schellart, W. P., and L. Moresi (2013), A new driving mechanism for backarc extension and backarc shortening through slab sinking induced toroidal and poloidal mantle flow: Results from dynamic subduction models with an overriding plate, *J. Geophys. Res. Solid Earth*, *118*, 3221–3248, doi:10.1002/jgrb.50173.

Schellart, W. P., M. W. Jessell, and G. S. Lister (2003), Asymmetric deformation in the backarc region of the kuril arc, northwest pacific: New insights from analogue modeling, *Tectonics*, *22*(5), doi:10.1029/2002TC001473.

Schenker, F., T. Gerya, and J.-P. Burg (2012), Bimodal behavior of extended continental lithosphere: Modeling insight and application to thermal history of migmatitic core complexes, *Tectonophysics*, *579*, 88–103, doi:10.1016/j.tecto.2012.07.002.

Sokoutis, D., J.-P. Brun, J. van den Driessche, and S. Pavlides (1993), A major OligoMiocene detachment in southern Rhodope controlling north Aegean extension, *J. Geol. Soc. London*, *150*, 243–246.

Sokoutis, D., J.-P. Burg, M. Bonini, G. Corti, and S. Cloetingh (2005), Lithospheric-scale structures from the perspective of analogue continental collision, *Tectonophysics*, *406*, 1–15, doi:10.1016/j.tecto.2005.05.025.

Stampfli, G., and G. Borel (2002), A plate tectonic model for the Paleozoic and Mesozoic constrained by dynamic plate boundaries and restored synthetic oceanic isochrons, *Earth Planet. Sci. Lett.*, *196*(1–2), 17–33, doi:10.1016/S0012-821X(01)00588-X.

Thielicke, W., and Stamhuis, E., 2014, PIVlab—Time-Resolved Digital Particle Image VelocimetryTool for MATLAB (version: 1.35), doi:10.6084/m9figshare.1092508.

Tirel, C., J.-P. Brun, and E. Burov (2004a), Thermomechanical modeling of extensional gneiss domes special publication, *Geol. Soc. Am.*, *380*, 67–78.

Tirel, C., F. Gueydan, C. Tiberi, and J.-P. Brun (2004b), Aegean crustal thickness inferred from gravity inversion: Geodynamical implications, *Earth Planet. Sci. Lett.*, *228*, 267–280, doi:10.1016/j.epsl.2004.10.023.

Tirel, C., J.-P. Brun, and D. Sokoutis (2006), Extension of thickened and hot lithospheres: Inferences from laboratory modeling, *Tectonics*, *25*, doi:10.1029/2005TC001804.

Tirel, C., J.-P. Brun, and E. Burov (2008), Dynamics and structural development of metamorphic core complexes, *J. Geophys. Res.*, *113*, doi:10.1029/2005JB003694.

Tirel, C., P. Gautier, D. J. J. van Hinsbergen, and M. J. R. Wortel (2009), Sequential development of interfering metamorphic core complexes: Numerical experiments and comparison with the cyclades Greece, *Geol. Soc. Spec. Publ.*, *311*, 257–292, doi:10.1144/SP311.10.

Tirel, C., J.-P. Brun, E. Burov, M. Wortel, and S. Lebedev (2013), A plate tectonics oddity: Caterpillar-walk exhumation of subducted continental crust, *Geology*, *41*, 555–558, doi:10.1130/G33862.1.

Tucholke, B. E., and J. Lin (1994), A geological model for the structure of ridge segments in slow spreading ocean crust, *J. Geophys. Res.*, *99*(B6), 11,937–11,958, doi:10.1029/94JB00338.

Turpaud, P., and T. Reischmann (2010), Characterisation of igneous terranes by zircon dating: Implications for UHP occurrences and suture identification in the Central Rhodope, northern Greece, *Int. J. Earth Sci. (Geol. Rundsch.)*, *99*, 567–591, doi:10.1007/s00531-008-0409-x.

van den Driessche, J., and J.-P. Brun (1989), Un modele cinematique de l'extension paleozoique superieur dans le sud du massif central, *C. R. Seances Acad. Sci., Vie Acad. Paris*, *309*, 1607–1613.

van Hinsbergen, D. J. J., E. Hafkenscheid, W. Spakman, J. E. Meulenkamp, and R. Wortel (2005a), Nappe stacking resulting from subduction of oceanic and continental lithosphere below Greece, *Geology*, *33*, 325–328, doi:10.1130/G20878.1.

van Hinsbergen, D. J. J., C. G. Langereis, and J. E. Meulenkamp (2005b), Revision of the timing, magnitude and distribution of Neogene rotations in the western Aegean region, *Tectonophysics*, *396*, 1–34, doi:10.1016/j.tecto.2004.10.001.

Wernicke, B. (1981), Low-angle normal faults in the basin and range Province: Nappe tectonics in an extending orogen, *Nature*, *291*, 645–648, doi:10.1038/291645a0.

Wernicke, B. (1985), Uniform-sense normal simple shear of the continental lithosphere, *Can. J. Earth Sci.*, *22*(1), 108–125, doi:10.1139/e85-009.

Whitney, D. L., C. Teyssier, P. Rey, and W. R. Buck (2013), Continental and oceanic core complexes, *Geol. Soc. Am. Bull.*, *125*, 273–298, doi:10.1130/B30754.1.

Wijns, C., R. Weinberg, K. Gessner, and L. Moresi (2005), Mode of crustal extension determined by rheological layering, *Earth Planet. Sci. Lett.*, *236*, 120–134, doi:10.1016/j.epsl.2005.05.030.